NAVAL POSTGRADUATE SCHOOL

MONTEREY, CALIFORNIA

THESIS

SURFACE WIND FIELD ANALYSES OF TROPICAL CYCLONES IN THE WESTERN PACIFIC

by

Louis J Cascino

September 2012

Thesis Advisor:	Patrick A. Harr
Second Reader:	Russell L. Elsberry

Approved for public release; distribution is unlimited

THIS PAGE INTENTIONALLY LEFT BLANK

REPORT DOCUMENTATION PAGE			Form Approved OMB No. 0704-0188
Public reporting burden for this collection of information is estimated to average 1 hour per response, including the time for reviewing instruction, searching existing data sources, gathering and maintaining the data needed, and completing and reviewing the collection of information. Send comments regarding this burden estimate or any other aspect of this collection of information, including suggestions for reducing this burden, to Washington headquarters Services, Directorate for Information Operations and Reports, 1215 Jefferson Davis Highway, Suite 1204, Arlington, VA 22202-4302, and to the Office of Management and Budget, Paperwork Reduction Project (0704-0188) Washington DC 20503.			
1. AGENCY USE ONLY ***(Leave blank)***	**2. REPORT DATE** September 2012	**3. REPORT TYPE AND DATES COVERED** Master's Thesis	
4. TITLE AND SUBTITLE Surface Wind Field Analyses of Tropical Cyclones in the Western Pacific		**5. FUNDING NUMBERS**	
6. AUTHOR(S) Louis J. Cascino			
7. PERFORMING ORGANIZATION NAME(S) AND ADDRESS(ES) Naval Postgraduate School Monterey, CA 93943-5000		**8. PERFORMING ORGANIZATION REPORT NUMBER**	
9. SPONSORING /MONITORING AGENCY NAME(S) AND ADDRESS(ES) N/A		**10. SPONSORING/MONITORING AGENCY REPORT NUMBER**	
11. SUPPLEMENTARY NOTES The views expressed in this thesis are those of the author and do not reflect the official policy or position of the Department of Defense or the U.S. Government. IRB Protocol number _____N/A_____.			
12a. DISTRIBUTION / AVAILABILITY STATEMENT Approved for public release; distribution is unlimited		**12b. DISTRIBUTION CODE** A	

13. ABSTRACT (maximum 200 words)

Surface wind characteristics inside mature Tropical Cyclones (TC) over the Western North Pacific (WPAC) are analyzed using *in-situ* observations from the Impact of Typhoons on the Ocean in the Pacific (ITOP 2010) field program. Surface wind speeds obtained from the Stepped Frequency Microwave Radiometer (SFMR) and GPS dropwindsondes were used to calculate four surface wind variables: lowest 150 m average wind speeds (WL150), Vsfc, 10-m interpolated wind speed, and SFMR surface wind speeds. Regression analysis is used to establish the consistency for each measured value to estimate the one-minute averaged surface wind speed. Results compared favorably to those computed for large data sets obtained in TCs over the Atlantic. These comparisons support and validate the accuracy of the SFMR wind speed measurements in the WPAC.

14. SUBJECT TERMS Tropical Cyclone Winds, Stepped Frequency Microwave Radiometer, GPS Dropwindsondes, Surface wind analysis, Lowest 150 m averaged wind speeds (WL150), 10-m interpolated wind speed			**15. NUMBER OF PAGES** 97
			16. PRICE CODE
17. SECURITY CLASSIFICATION OF REPORT Unclassified	**18. SECURITY CLASSIFICATION OF THIS PAGE** Unclassified	**19. SECURITY CLASSIFICATION OF ABSTRACT** Unclassified	**20. LIMITATION OF ABSTRACT** UU

NSN 7540-01-280-5500 Standard Form 298 (Rev. 2-89)
Prescribed by ANSI Std. 239-18

THIS PAGE INTENTIONALLY LEFT BLANK

Approved for public release; distribution is unlimited

SURFACE WIND FIELD ANALYSES OF TROPICAL CYCLONES IN THE WESTERN PACIFIC

Louis J. Cascino
Second Lieutenant, United States Air Force
B.S., United States Air Force Academy, 2011

Submitted in partial fulfillment of the
requirements for the degree of

MASTER OF SCIENCE IN METEOROLOGY

from the

NAVAL POSTGRADUATE SCHOOL
September 2012

Author: Louis J. Cascino

Dr. Patrick A. Harr
Thesis Advisor

Dr. Russell L. Elsberry
Second Reader

Dr. Wendell Nuss
Chair, Department of Meteorology

THIS PAGE INTENTIONALLY LEFT BLANK

ABSTRACT

Surface wind characteristics inside mature Tropical Cyclones (TC) over the Western North Pacific (WPAC) are analyzed using *in-situ* observations from the Impact of Typhoons on the Ocean in the Pacific (ITOP 2010) field program. Surface wind speeds obtained from the Stepped Frequency Microwave Radiometer (SFMR) and GPS dropwindsondes were used to calculate four surface wind variables: lowest 150 m average wind speeds (WL150), Vsfc, 10-m interpolated wind speed, and SFMR surface wind speeds. Regression analysis is used to establish the consistency for each measured value to estimate the one-minute averaged surface wind speed. Results compared favorably to those computed for large data sets obtained in TCs over the Atlantic. These comparisons support and validate the accuracy of the SFMR wind speed measurements in the WPAC.

THIS PAGE INTENTIONALLY LEFT BLANK

TABLE OF CONTENTS

LIST OF FIGURES

LIST OF TABLES

THIS PAGE INTENTIONALLY LEFT BLANK

LIST OF ACRONYMS AND ABBREVIATIONS

AOC:	Air Operations Center
AVAPS:	Airborne Vertical Atmospheric Profiling System
DOTSTAR:	Taiwanese Reconnaissance aircraft
ETT:	Extra-Tropical Transition
hPa:	Hectopascals
HRD:	Hurricane Research Division
ITOP:	Impact of Typhoons on the Ocean in the Pacific
IR:	Infrared
JTWC:	Joint Typhoon Warning Center
KT:	Knots
LLCC:	Low-Level Convection Center
MSLP:	Minimum Sea Level Pressure
NCAR:	National Center for Atmospheric Research
NHC:	National Hurricane Center
n mi:	Nautical mile
NOAA:	National Oceanic and Atmospheric Administration
NRL:	Navy Research Lab
RMW:	Radius of Max Wind
SFC:	Surface
SFMR:	Stepped Frequency Microwave Radiometer
SST:	Sea-Surface Temperature
STY:	Super Typhoon
TC:	Tropical Cyclone
TCFA:	Tropical Cyclone Formation Alert
TCS-08:	Tropical Cyclone Structure-08
TD:	Tropical Depression
THORPEX:	The Observing System Research and Predictability Experiment
TPARC:	THORPEX Pacific Asian Regional Campaigns

TS:	Tropical Storm
TUTT:	Tropical Upper Tropospheric Trough
TY:	Typhoon
US:	United States
Vsfc:	Surface Wind Speed
WL150:	Mean winds in the lowest 150 m of a dropwindsonde
WPAC:	Western North Pacific

ACKNOWLEDGMENTS

I would like to thank my parents for their unwavering support through my whole life and for listening to all of my complaints while finishing up my thesis. To my classmates Chandra, Steph, Nick, Paul, Sean, and Dan, it was awesome getting to know all of you, and I will not forget the leadership insight you gave me. To my officemates Dave and Rob, we had fun fighting through the thesis process with our wonderful advisor! Professor Harr, thank you very much for dealing with all of my nagging questions and helping me get my degree completed in one year. Professor Elsberry, thank you for your help with finalizing my edits. To all of my professors, thank you for your great instruction and guidance, I was honored to be in your classes. To my fellow LTs (Zack, Kellan, and Ashleigh), I am glad you guys kept me on track, if it weren't for you I probably wouldn't have gone to any of our mandatory functions. I hope you guys kill it in your future careers! To Paul Homan, my first Meteorology teacher, it was through your dedication and help that I was able to get my scholarship, thank you for all of your hard work, without it I would not have had this awesome opportunity. I am thankful for all of the awesome experiences that I have had out here in Monterey, it has been a great year!

THIS PAGE INTENTIONALLY LEFT BLANK

I. INTRODUCTION

A. MOTIVATION

Tropical Cyclones (TCs) are one of the most severe weather phenomena to occur over oceanic and coastal regions. These warm-core, low-pressure systems produce devastating winds, significant wave heights, and torrential rain. When these storms strike land, they often cause widespread devastation. Normally, TCs form slightly away from the equator in the warm, moist atmospheric conditions that exist over tropical oceans. Warm water is essential for the formation and intensification of these storms as it represents a source of potential energy (Gray 1968). General guidelines for TC formation (Gray 1968) are sea-surface temperatures (SSTs) greater than 26^{o}C, unstable atmospheric conditions, a moist mid-troposphere, and weak vertical wind shear. Over oceanic regions, these conditions often occur over data-sparse regions. Therefore, it is difficult to obtain adequate *in-situ* observations of processes related to TC formation and intensification. Although global satellite coverage is currently at an all time maximum, there is often a lack of data over the environment of a mature TC. It is for this reason that National Oceanic and Atmospheric Administration (NOAA) and the United States Air Force (USAF) conduct research and reconnaissance aircraft missions into TCs that threaten landfall over the United States. During these missions, atmospheric and oceanic data are collected from a variety of observing platforms. Flight-level observations include wind speed and direction, temperature, pressure, and moisture (Hock and Franklin 1999). The GPS dropwindsonde provides a vertical profile of pressure, temperature, humidity, and wind speed and direction (Hock and Franklin 1999). The SFMR instrument is used to estimate surface wind speeds (Uhlhorn et al. 2007).

Using data obtained in the Tropical Cyclone Structure 2008 (TCS-08) and The Observing System Research and Predictability Experiment (THORPEX) Pacific Asian Regional Campaign (T-PARC), Havel (2009) compared surface wind speed observations obtained by GPS dropwindsondes and the SFMR. The conclusion was a high correlation existed between wind speeds from these TCS-08/T-PARC measurements for the five TCs examined.

Prior to the implementation of the SFMR on operational weather reconnaissance aircraft, the ratio between surface wind speeds obtained from dropwindsondes and flight-level wind speed was used to map the surface wind field during reconnaissance missions (Franklin et al. 2003 and Powell et al. 2004). Over the Atlantic, the ratio of flight-level and surface winds was found to vary from 0.80 to 0.93. Powell et al. (2009) examined the sensitivity of the ratio to the vertical slant between the radius of maximum winds (RMW) at flight level and at the surface. Using aircraft measurements from the T-PARC/TCS-08 field program over the Western North Pacific, Havel (2009) also defined a slant reduction factor that compared flight-level winds to the surface winds. This reduction factor for TCs in the Pacific was found to compare well with the reduction factor calculated for TCs in the Atlantic (Powell et al. 2009, Franklin 2011). Heck (2011) added to the analyses by Havel (2009) by analyzing two TCs from the Impact of Typhoons on the Ocean in the Pacific (ITOP) project conducted in 2010.

To expand on the Havel (2009) and Heck (2011) studies that defined the relationship between flight-level winds and surface winds, this thesis examines the characteristics of vertical wind variations between the flight-level and the surface. Variations in vertical profiles are also examined in relation to the location of the flight-level RMW. In this thesis, three typhoons observed during ITOP are studied. A unique aspect of these TCs is that they represent a spectrum of typhoon characteristics that typically occur over the WPAC. Typhoon (TY) Fanapi was a near-average storm in terms of intensity and size. TY Malakas was a large storm with a broad structure. Supertyphoon Megi was a very intense, small storm.

Examination of surface wind fields for these three storms will allow TC forecasters to be better equipped to forecast the size and intensity of TCs in the WPAC, which will improve resource protection of US military assets over the WPAC. Finally, the understanding of boundary layer structure in a mature TC will be increased.

B. WESTERN NORTH PACIFIC TROPICAL CYCLONES

Although TCs occur over the majority of tropical ocean basins (Figure 1), there are variations in intensity, frequency, and seasonality. Of all the tropical ocean basins, the WPAC has the highest frequency of occurrence and largest number of intense TCs. A

unique characteristic of WPAC TC activity is that a TC may occur during any month (Figure 2) as a result of favorable environmental conditions that exist through all four seasons. As defined above, these favorable conditions are: sufficient ocean thermal energy (SST>26^{o}C to a depth of 60 m), increased mid-troposphere moisture, atmosphere vertical instability, enhanced relative vorticity in the lower troposphere, weak vertical wind shear, and displacement from the equator by at least 5^{o} of latitude (Gray 1968). During 2010, only 19 TCs occurred over the WPAC, which was far less than the average of 31 TCs. As defined by the Joint Typhoon Warning Center (JTWC), TC intensity is determined by the surface (10 m) wind speed. A Tropical Depression (TD) has winds between 25–33 kt, Tropical Storm (TS) speeds are between 34 and 63 kt, Typhoon (TY) winds are greater than or equal to 64 kt. The wind speeds used to determine intensity are the maximum one-minute mean sustained 10-m wind speed. In this study, a mature storm is defined as a TC that is at least TY strength.

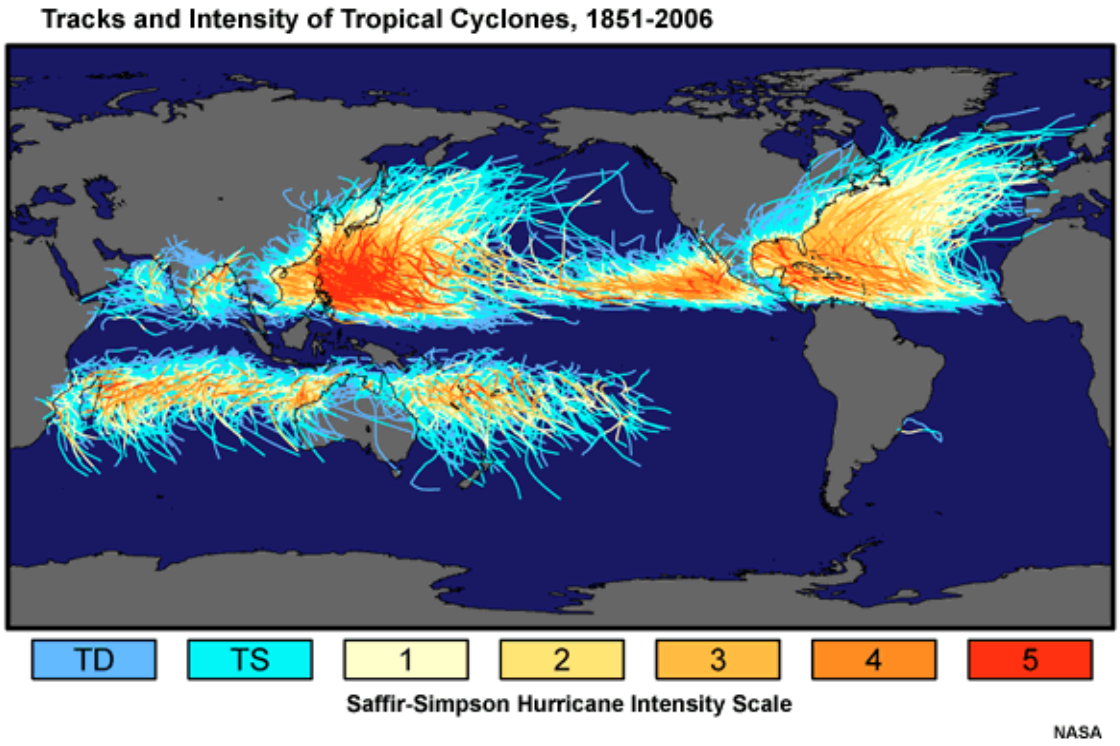

Figure 1. Global distribution of observed tropical cyclone tracks from 1851–2006. (From: Comet 2009)

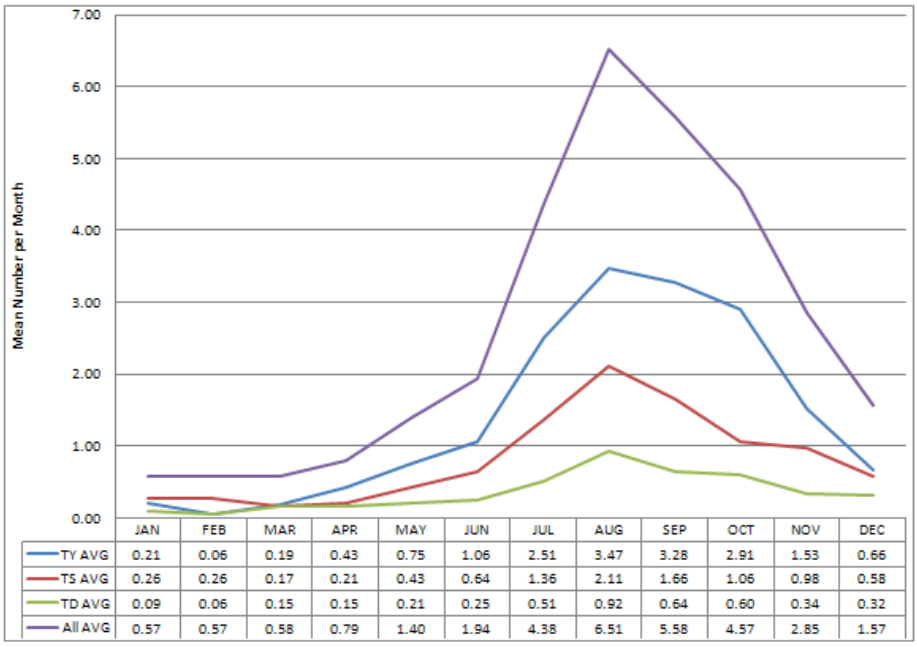

	JAN	FEB	MAR	APR	MAY	JUN	JUL	AUG	SEP	OCT	NOV	DEC
TY AVG	0.21	0.06	0.19	0.43	0.75	1.06	2.51	3.47	3.28	2.91	1.53	0.66
TS AVG	0.26	0.26	0.17	0.21	0.43	0.64	1.36	2.11	1.66	1.06	0.98	0.58
TD AVG	0.09	0.06	0.15	0.15	0.21	0.25	0.51	0.92	0.64	0.60	0.34	0.32
All AVG	0.57	0.57	0.58	0.79	1.40	1.94	4.38	6.51	5.58	4.57	2.85	1.57

Figure 2. Average number of WPAC TCs of all intensities by month 1959–2011. (From: JTWC 2011)

Over the WPAC, the majority of storms form west of the date line, and track toward the west-northwest under the influence of deep-layer mean easterly winds. The low-level easterly winds define the boundary between a monsoon trough to the south and a subtropical ridge to the north. As the TCs move farther west, their mean motion often depends on the relative strength of the subtropical ridge and monsoon trough. During the months of June – October, which is the peak season for the WPAC (Figure 2), storms often recurve to the north and move toward the islands of Japan. Recurvature tends to result when the subtropical ridge is weak. Storms that form outside of the peak season often move farther westward as the subtropical ridge dominates the WPAC as the monsoon trough retreats toward the west.

C. IMPACT OF TYPHOONS ON THE OCEAN IN THE PACIFIC (ITOP) PROGRAM

The ITOP program was a multi-national field program that sought to increase understanding of interactions between TCs and the ocean over the WPAC. Research observing platforms for ITOP included the WC-130J aircraft from the 53rd Air Force

Reserve Hurricane-Hunter Squadron (Figure 3a), DOTSTAR reconnaissance aircraft from Taiwan (Figure 3b), and the Research Vessel (RV) Revelle from the University-National Oceanographic Laboratory System (UNOLS) research ship (Figure 3c). Data sources included air-deployed floats and drifters, gliders, moored buoy arrays, GPS dropwindsondes, satellites, and model-derived forecasts (Figure 4). The research goals of the ITOP program were to: 1) Define how the ocean cold wake forms and dissipates; 2) Observe the air-sea fluxes for winds greater than 30 m s^{-1}; 3) Examine how ocean eddies affect typhoon intensity; 4) Examine the surface wave field under typhoons; and 5) Examine typhoon formation in relation to environmental factors. During the field phase of ITOP, approximately 250 aircraft flight hours were used and roughly 750 dropwindsondes were deployed.

Figure 3. Images of the basic observational platform used in the ITOP program. (a) WC-130J (b) DOTSTAR and (c) Research Vessel Revelle UNOLS. (From: ITOP 2010)

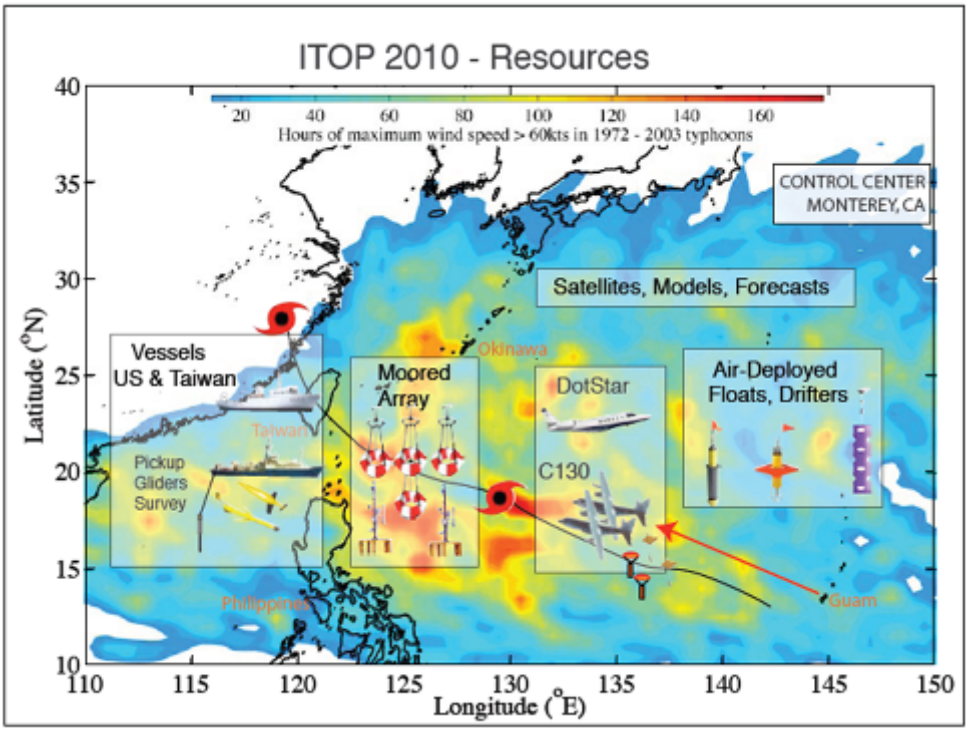

Figure 4. Depiction of ITOP resources and their relative locations in the WPAC. (From: ITOP 2010)

During ITOP, three mature TCs formed over the WPAC: TY Fanapi, TY Malakas and TY Megi (Table 1). Observations in these storms were collected using the multiple observing platforms identified above. Of particular interest for this thesis are the observations obtained from the WC-130J flight-level recordings and GPS dropwindsondes.

D. SYNOPTIC OVERVIEW

During 2010, there was a significant decrease in the number of TCs compared to the average. This was a rather anomalous season with a weak monsoon trough and enhanced easterly trade winds, which are typical of La Nina conditions. Of the 19 storms that occurred, 14 reached TS stage and of these 14 storms, eight reached TY strength (JTWC 2010).

Table 1. Tropical Cyclones that occurred during ITOP (From: JTWC 2010).

TC	NAME	PERIOD	EST MAX SFC WINDS (KT)	Minimum MSLP (hPa)
TY 12W	Fanapi	14 – 20 Sep	105	944
TY 13W	Malakas	20–25 Sep	90	956
STY 15W	Megi	13–23 Oct	160	903

1. Typhoon Fanapi

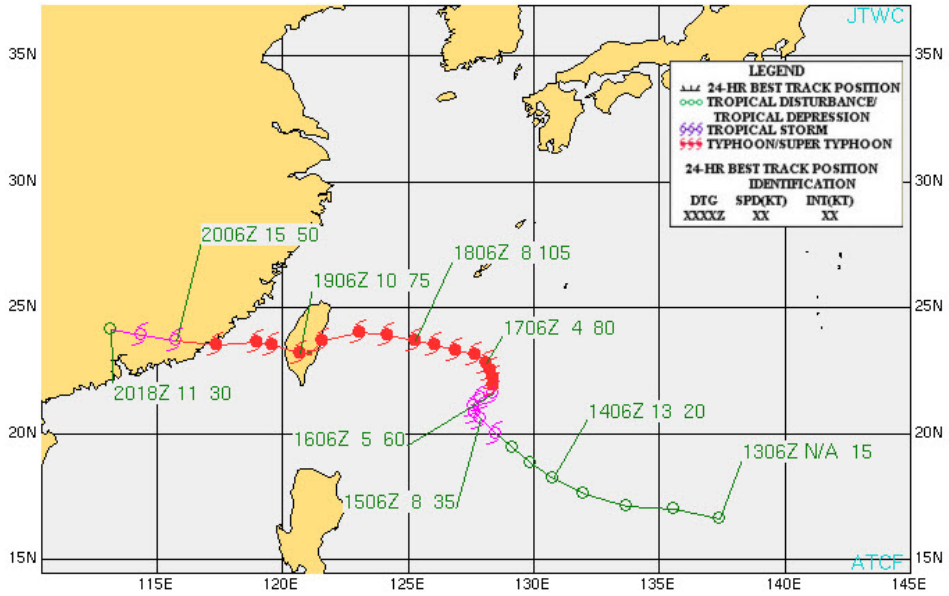

Figure 5. The best track of Typhoon Fanapi (TY 12W) (From: JTWC 2010).

Typhoon Fanapi (Figure 5) was the twelfth storm to form during the 2010 TC season in the WPAC. This storm was initially reported as a TD on 14 September 2010 when it was located at approximately 16.5°N 137.5°E (Figure 6a). The TD was in an area of favorable low wind shear that allowed for the intensification into TS strength on 0600 UTC 16 September (Figure 6b). Fanapi was upgraded to TY intensity at 0600 UTC 17 September (Figure 6c). During the intensification from TS stage to TY stage, the translational speed of Fanapi slowed as the storm began a slow turn to the north-northeast

in response to the weakening of the subtropical ridge under the influence of a mid-level trough. Fanapi curved back to the west (Figure 5) toward Taiwan as the ridge strengthened. The maximum intensity occurred on 18 September (Figure 6d) with surface one-minute averaged winds of 105 kt. After TY Fanapi made landfall over Taiwan on 19 September, it weakened and was downgraded to a TS on 20 September as it made landfall over China.

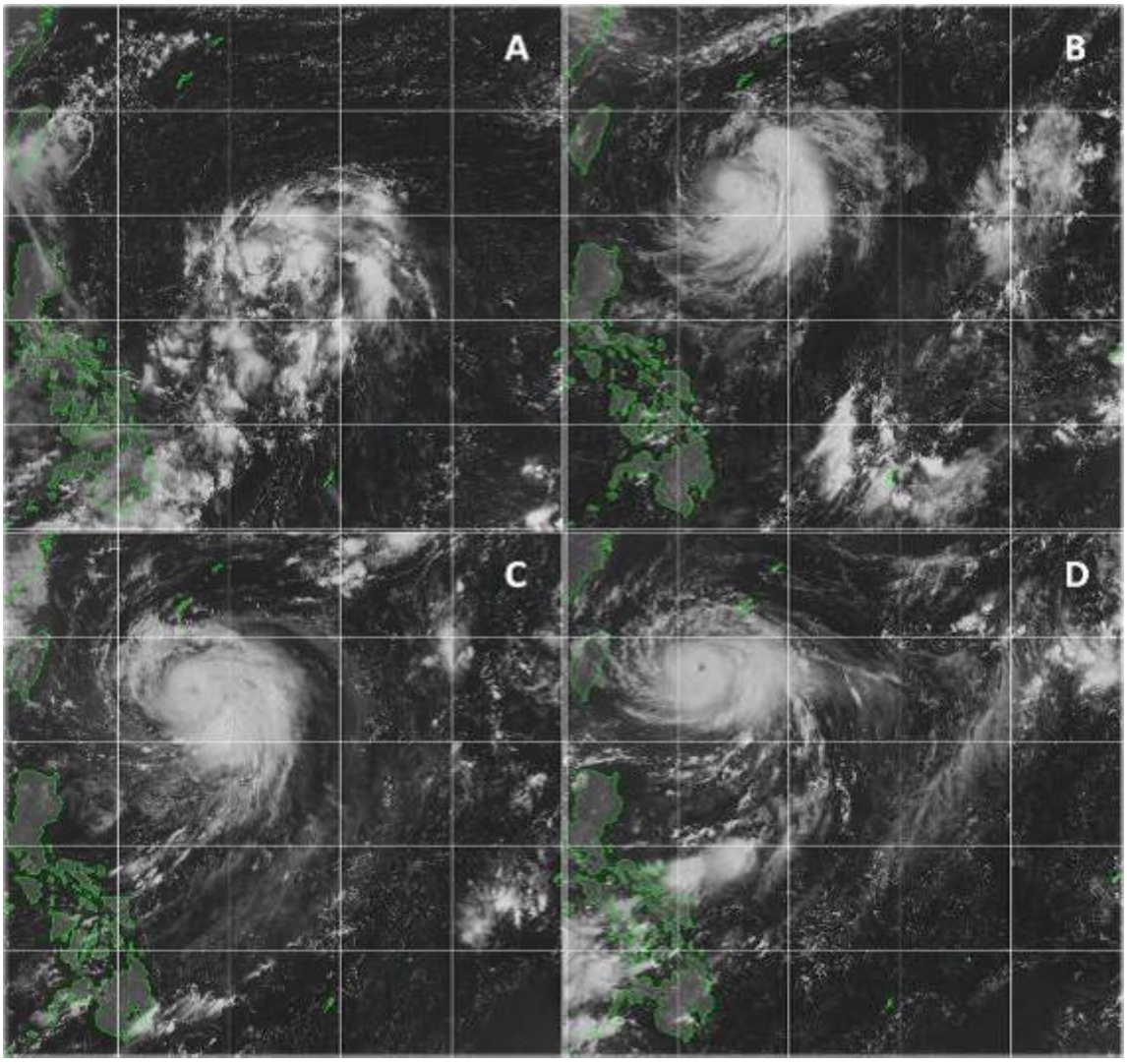

Figure 6. Visible satellite imagery for TC Fanapi at a) TD strength at 0032 UTC 14 September; b) TS strength at 0032 UTC 16 September; c) TY strength at 0032 UTC 17 September; and d) Maximum intensity at 0032 UTC 18 September.

2. Typhoon Malakas

The next ITOP 2010 typhoon examined was TY Malakas (Figure 7). A TCFA was issued for TC Malakas on 0300 UTC 19 September. At this time, the pre-Malakas disturbance was located 205 n mi off Saipan moving to the northwest at approximately 8 kt. The first TC warning for Malakas was issued on 0600 UTC 20 September (Figure 8a). At this time, an upper-level anticyclone created favorable outflow conditions for the storm. This outflow interacted with a TUTT to the north of the system and contributed to the intensification of the storm. At 0000 UTC 22 September (Figure 8b) the storm was upgraded to TS strength with a surface one-minute averaged wind speed of 30 kt (Figure 7). At this time the storm motion was still to the northwest. As a result of the interaction with a mid-latitude upper-level trough, the subtropical ridge weakened and the TS began to move poleward. Strong vertical wind shear from the north impeded the intensification of TS Malakas and exposed the well-defined LLCC (Figure 8b) as the bulk of the convection occurred to the south of the LLCC. At approximately 1200 UTC 22 September, TS Malakas was upgraded to TY strength with a maximum wind speed of 65 kt. At this time, Malakas was located approximately 295 n mi south of Iwo To, Japan (Figure 7). Due to increased vertical wind shear, TY Malakas was downgraded to TS on 0900 UTC 23 September. At 2053 UTC 23 September, it was apparent that upper-level subsidence decreased and Malakas re-intensified by 10 kt over a six-hour period. While moving rapidly northward, the maximum winds of TY Malakas were estimated to be 90 kt and the MSLP was 956 hPa (Table 1) on 1200 UTC 24 September (Figure 8c). The last warning for TY Malakas was issued on 0300 UTC 25 September (Figure 8d). At this time, TY Malakas was starting the process of extratropical transition (ETT) into an intense mid-latitude low pressure system.

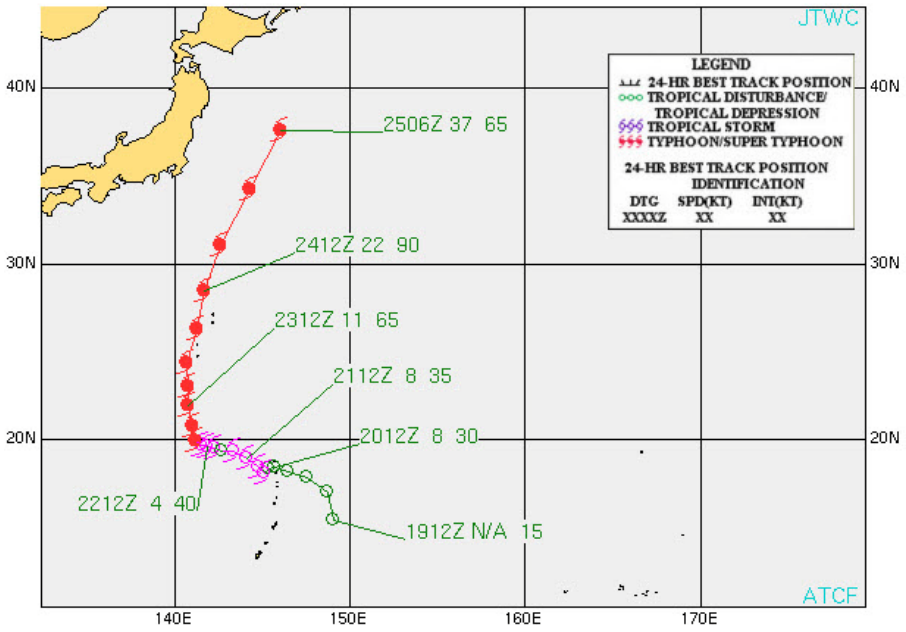

Figure 7. The best track of Typhoon Malakas (TY 13W) (From: JTWC 2010).

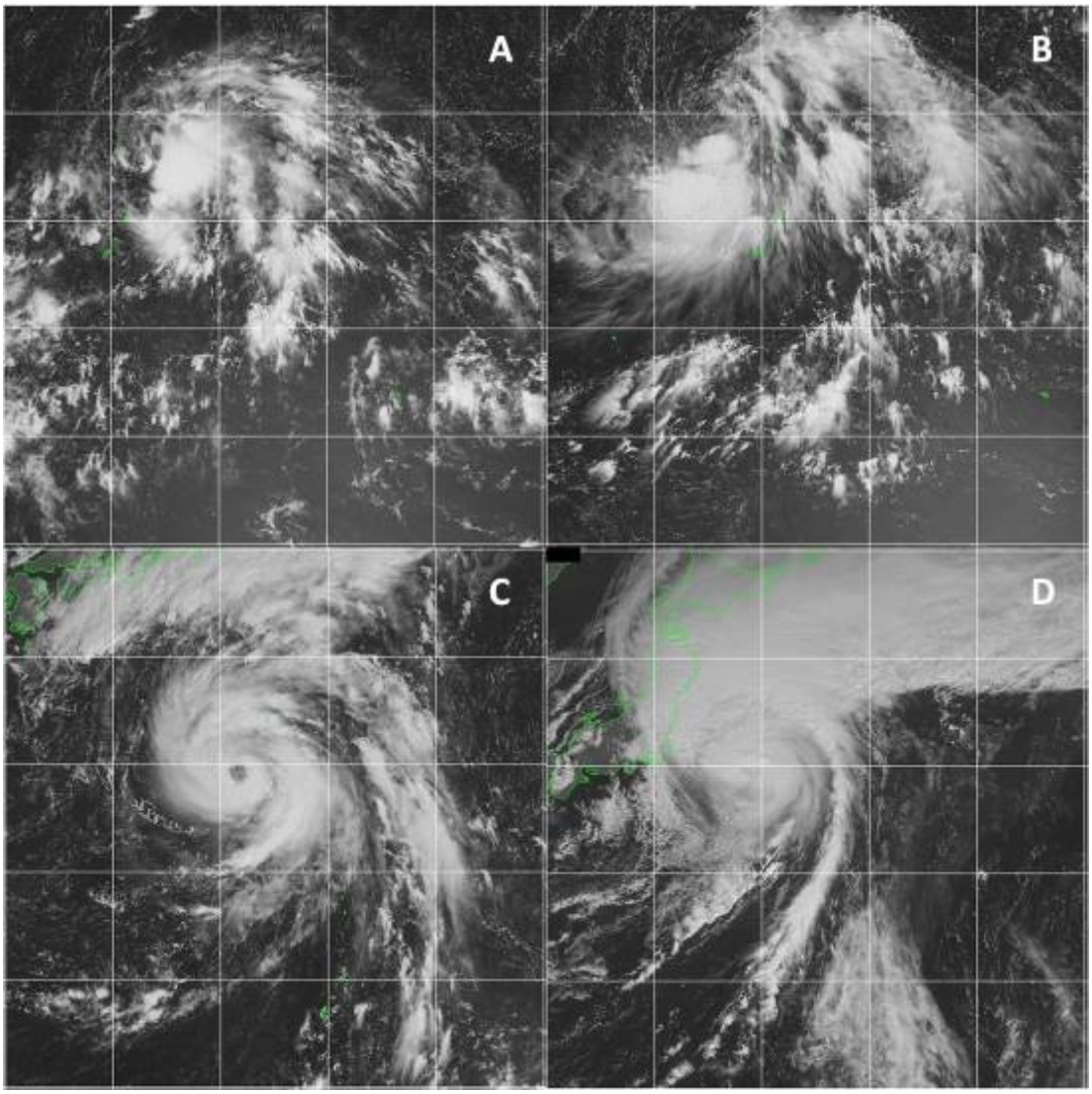

Figure 8. Visible satellite imagery for TY Malakas at a) TD strength at 0032 UTC 20 September; b) TS strength at 0032 UTC 22 September; c) TY strength at 0032 UTC 24 September; and d) starting ETT at 0032 UTC 25 September.

3. Typhoon Megi

The first TCFA issued for the pre-Megi disturbance was at 0900 UTC 12 October (Figure 9). As a TD, the pre-Megi disturbance was an area of organized convection that existed approximately 260 n mi west of Guam (Figure 10a). At 1200 UTC 13 October TD 15W was upgraded to TS and named Megi (Figure 9). The storm initially tracked to the northwest and intensified into a TY at 1200 UTC 14 October with one-minute averaged surface wind speeds estimated at 70 kt. By 0000 UTC 15 October (Figure 10b),

TY Megi was a strong storm with maximum winds of 90 kt. Megi continued to move to the northwest and over the ensuing two days wind speeds increased by 40 kt. On 16 October (Figure 10c), TY Megi changed direction from northwesterly to west-southwesterly (Figure 9). Megi continued to intensify beyond 115 kt, and at 0240 UTC 17 October (Figure 10d) it reached maximum intensity of 160 kt with a MSLP of 903 hPa (Table 1). STY Megi made landfall on the island of Luzon in the Philippines between 0300–0600 UTC 18 October (Figure 10e). The storm weakened over land and then re-intensified as it entered the South China Sea (Figure 10f). On 19 September, TY Megi recurved to the north (Figure 9) and slowly weakened as it tracked toward China (Figure 10g).

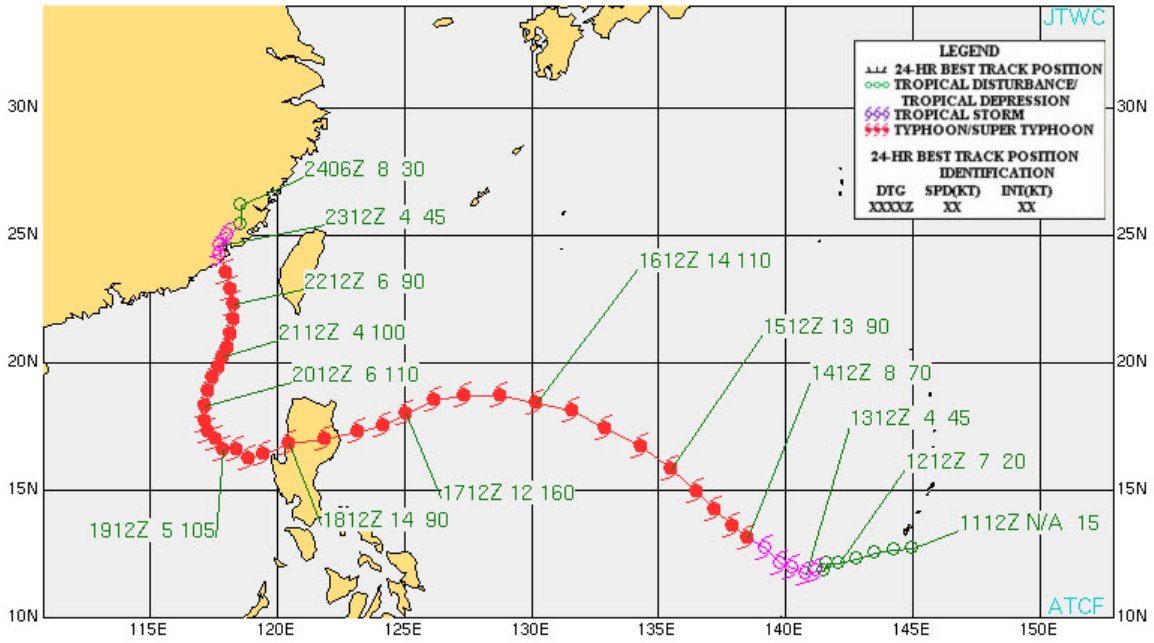

Figure 9. The best track of Super typhoon Megi (TY 13W) (From: JTWC 2010).

Although the number of TCs that occurred during ITOP 2010 was well below the climatological average, these three storms exhibited a wide range of intensity and structural characteristics. Additionally, each storm existed over varied ocean and atmospheric conditions that are typical of the WPAC environment.

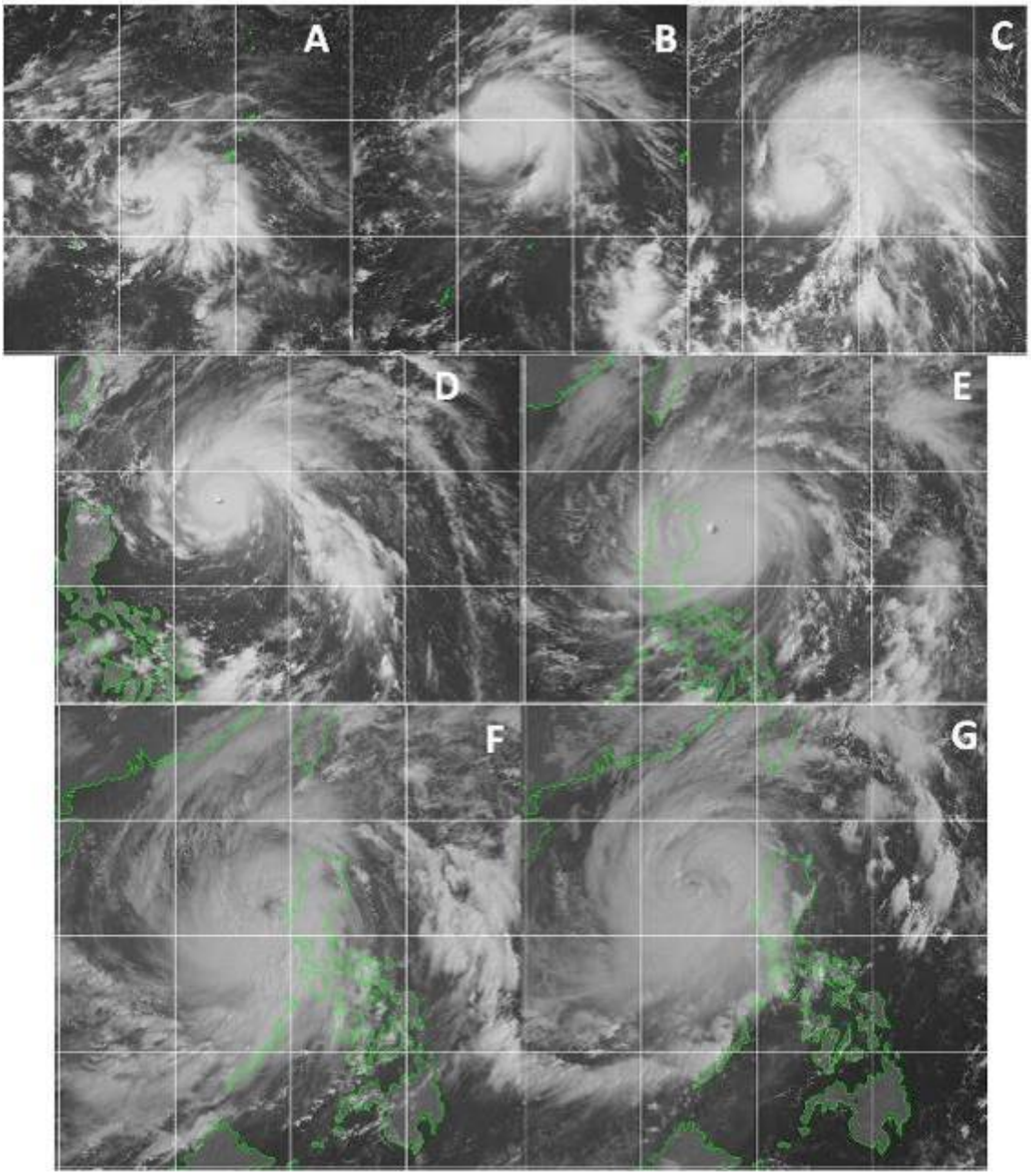

Figure 10. Visible satellite imagery for Typhoon Megi at a) TS strength at 0030 UTC 13 October; b) TY strength at 0030 UTC 15 October; c) at 0130 UTC 16 October; d) at 0130 UTC 17 October; e) Maximum intensity when Megi made landfall on the island of Luzon 18 October; f) TY Megi after crossing the island of Luzon 0030 UTC 19 October; and g) 0030 UTC 20 October.

II. METHODOLOGY

A. BACKGROUND

Observations of surface winds in a TC have always been extremely difficult to obtain due to the harsh conditions at the surface of these storms. Until recently, surface wind estimates were calculated using the "90% rule." This rule by Franklin et al. (2003) defined the surface wind as 90% of the flight-level winds at 700 hPa. With advances in remote sensing technology such as the SFMR and GPS dropwindsondes, the "90% rule" has been examined relative to surface wind speeds over both Atlantic and Pacific TCs (Powell et al. 2009; Havel 2009; Franklin 2011).

1. SFMR

The WC-130J aircraft that conducted the reconnaissance missions into the ITOP 2010 storms were equipped with a NOAA/Aircraft Operations Center (AOC) SFMR. This instrument estimates surface wind speed along the aircraft flight track. The SFMR is a passive microwave sensor that directly measures the amount of microwave energy emitted by sea foam (Powell et al. 2009). The algorithm used to estimate the surface wind speeds assumes that the amount of foam coverage on the sea surface increases monotonically with an increase in wind speed (Powell et al. 2009). Wind speeds less than 10 m s^{-1} are not calculated in the SFMR because the brightness temperature (Tb) is too small for the SFMR to define. Currently, the SFMR is the most reliable passive microwave sensor at measuring wind speeds > 20 m s^{-1} (Uhlhorn et al. 2007). However, the SFMR has been found to slightly underestimate wind speeds in high winds greater than 50 m s^{-1}(Uhlhorn et al. 2007). Uhlhorn and Black (2003) found that the main source of error in SFMR estimates of wind speeds was a result of inaccurate sea-surface temperature estimates in hurricanes. This resulted in an error in the geophysical model function (GMF) at speeds greater than 55 m s^{-1} (Uhlhorn et al. 2007) because the emissivity of sea foam at higher wind speeds varied more than at low to moderate speeds. Therefore, it was necessary to collect data sets with wind speeds greater than 50 m s^{-1}. In 2005, the abundance of collocated GPS dropwindsondes and SFMR observations over the

Atlantic allowed new estimates to reduce the error at high wind speeds. Currently, the SFMR emissivity-wind speed GMF is installed on all the Air Force WC-130J aircraft (Uhlhorn et al. 2007). The new NOAA/AOC SFMR-derived surface wind speed accuracy is estimated to be 2.2±0.4% in high wind speed regimes, which is a factor of two better than the Hurricane Research Divisions (HRD) SFMR (Uhlhorn et al. 2007).

2. WL150

Dropwindsondes equipped with GPS sensors have been released by the NOAA P-3 aircraft into TCs since 1997 (Hock and Franklin 1999). These measurement tools record multiple environmental parameters during the approximate 12-minute descent to the surface from 700 hPa. One important measurement made by the dropwindsondes is the wind speed and direction in the boundary layer. As the sonde descends, the data collection resolution is 0.5 s per sample, which provides for a typical 5 m vertical resolution (Hock and Franklin 1999). This sampling rate results in the lowest observational level of data recorded to typically be at or just below 10 m as the wind speed variations near the surface are too rapid to be measured by the sonde sampling rate (Hock and Franklin 1999).

One typical measure of the surface wind is the 10-m wind. However, the 10-m, or near-surface wind (U10) is only an instantaneous measurement in time. Thus, a 10-dropwindsonde wind is not equivalent to the one-minute averaged wind speed used by the NHC to characterize hurricane intensity (Uhlhorn et al. 2007). To compensate for the lack of an actual one-minute averaged surface wind speed, Franklin et al. (2003) proposed using the variable WL150, which is the average of the winds in the lowest 150 m layer, to represent the one-minute average wind speed.

The WL150 is used here to estimate a surface wind speed from the average of the lowest 150 m winds reported by the dropwindsonde. To extrapolate the winds to the surface, a statistical reduction was defined by Franklin et al. (2003) to adjust the WL150 to the surface wind (Figure 11). The ratio of 10-m surface wind speed to the WL150 is based on the mean altitude of the 150 m layer (Katzberg and Dunion 2009) and can be used to determine whether a dropwindsonde actually reported a 10-m wind speed. For

example, for a mean WL150 altitude of 85 m the WL150 and U10 ratio is 0.83 (Figure 11). Therefore any ratio of U10/WL150 that exceeds 0.83 has a 10-m wind reported.

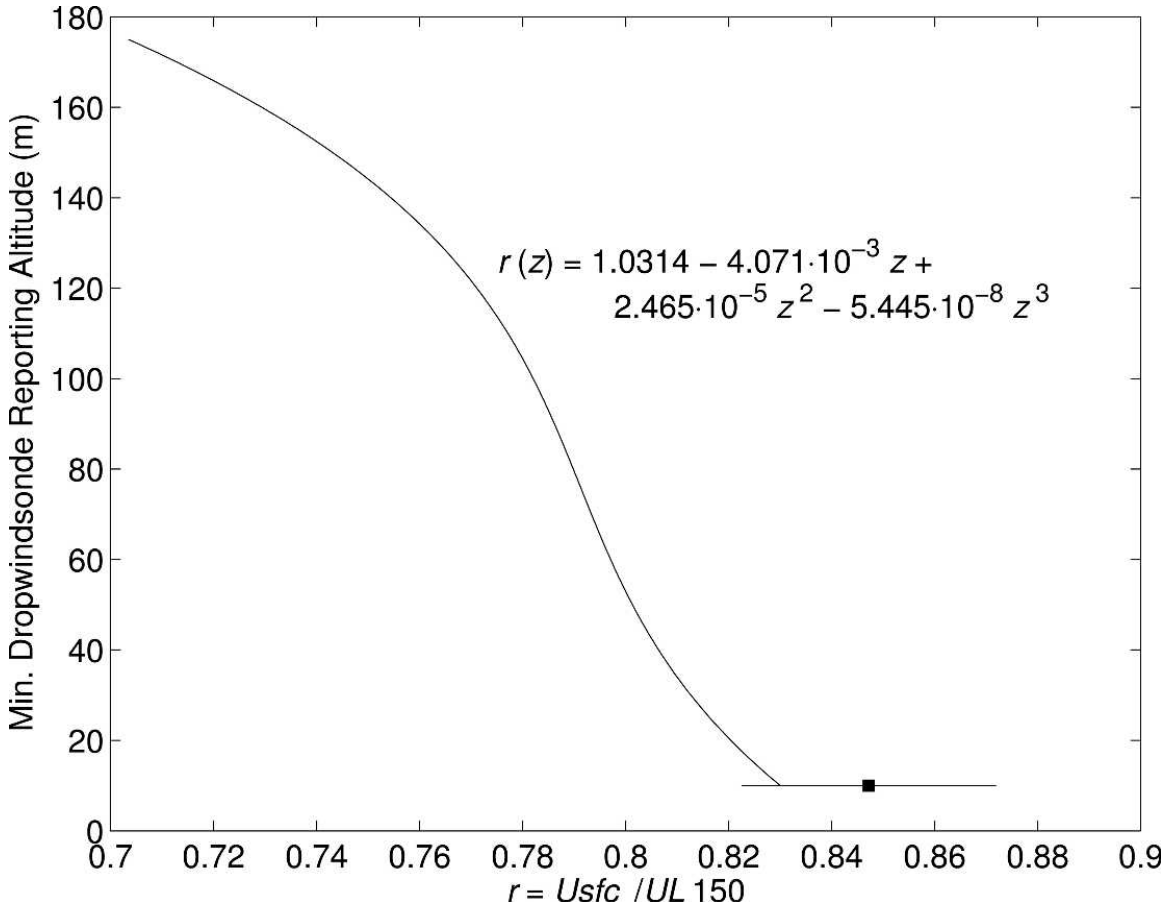

Figure 11. Ratio of GPS dropwindsonde near-surface wind speed (Vsfc) to the WL150 wind speed. This ratio is empirically determined from a mean eyewall profile created by Franklin et al. (2003) (From Uhlhorn et al. 2007).

B. DATA SOURCES

1. In-Situ Observations

During the ITOP 2010 experiment in the WPAC, *in-situ* observations were collected at flight-level using WC-130J aircraft. The vertical profiles of winds were measured by GPS dropwindsondes and the surface wind speeds were obtained by the SFMR. The data set used in this thesis consists of flight-level data and GPS

dropwindsondes from the ITOP 2010 field experiment. Observations from TY Fanapi, TY Malakas and TY Megi were analyzed in this thesis. Each aircraft mission was categorized as either a surveillance or reconnaissance type. In this thesis, only reconnaissance missions are analyzed as surveillance flights occurred prior to storm formation. Reconnaissance flights typically had 120 n mi radial legs that passed through the storm center. For the three storms of interest, dropwindsonde spacing ranged from 30–45 n mi along the 120 n mi radial legs. At the storm center and at the radius of maximum winds (RMW), there were often multiple sondes released in rapid succession. Data recorded by the dropwindsondes include pressure, dry bulb temperature, dew point temperature, relative humidity, wind direction and speed, altitude, and vertical wind speed. The NCAR dropwindsondes have an accuracy of 0.5–2.0 m s^{-1} for winds greater than 10 m s^{-1} (Hock and Franklin 1999).

Along with the SFMR data, the WC-130J flight-level data were recorded in the form of HDOBS. These data included flight-level pressure, latitude and longitude, wind direction and speed, temperature, dew point temperature, and geopotential altitude. For this study, the flight-level data were used with a 10-sec resolution.

The flight level for the TY Fanapi and TY Malakas missions was 10,000 ft. The flight level for STY Megi was increased to 12,000 ft as a result of a GPS reporting problem with the AVAPS dropwindsonde system.

2. Data Quality Control

Each GPS dropwindsonde data point was quality controlled by NCAR to determine whether various errors could have occurred during the sonde operation. Each dropwindsonde was first checked for full profiles of raw pressure, temperature, relative humidity, wind speed, and vertical fall rates to detect errors in the automatic launch detection on the dropwindsonde. The second check was to pass the data through a post-processor to smooth the profile and remove likely erroneous data. The data were then examined as time series plots of temperature, relative humidity, wind speed, and fall rate for consistency among the soundings from individual flights, and also to check for a "fast fall" that may have resulted from a faulty parachute deployment. This step also examined whether data were transmitted all the way to the surface.

These quality control measures resulted in the removal of 15 soundings due to lack of data or poor quality. As a result of a change in the Vaisala firmware, 27 files had significant noise in the raw profiles and were thus run through the post-processor program with increased smoothing parameters. An example of the original profiles before being run through the post-processor is displayed in Figure 12. A total of 14 soundings failed to report data to the surface and thus the geopotential altitudes for the vertical profile were calculated from flight level down. Dropwindsondes that fell at an accelerated rate were classified as "fast fall drops" and all wind data were removed. Out of the dataset 25 were classified as "fast fall drops" and 20 as "partial fast fall drops."

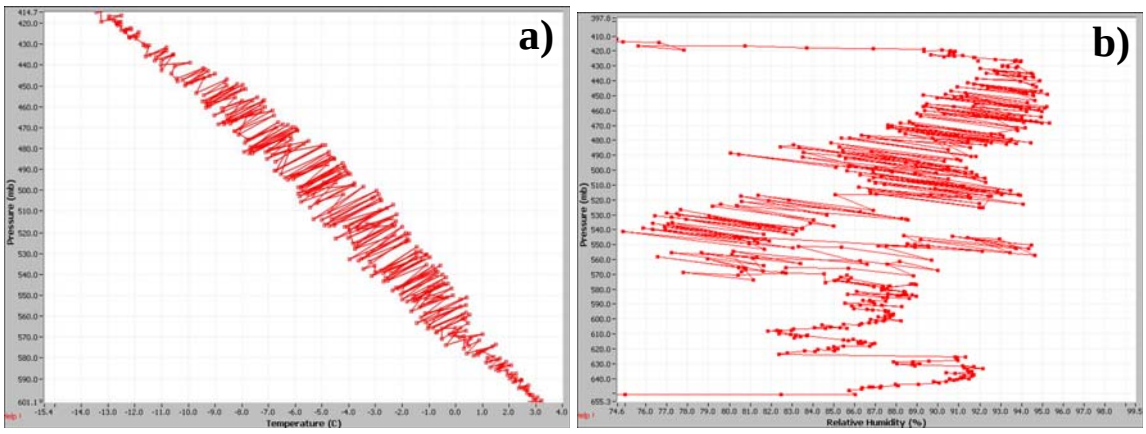

Figure 12. a) Profile of raw temperature versus pressure from file D20100828_203458, and b) profile of raw relative humidity versus pressure from file D20100828_203458. This image contains the oscillations that are smoothed by the post-processing program.

C. ANALYSIS METHODS

The flight level 10-s data were displayed in a storm-relative reference frame after linearly interpolating the storm center locations throughout the length of the mission at a resolution of every minute. The geographic flight-level locations were adjusted to be storm-relative by using a delta-latitude and delta-longitude correction relative to the storm center. The initial center fix was chosen based on the time of the first vortex message. Once the flight path was converted to storm-relative coordinates, the same

process was conducted for the location of the dropwindsondes. Plots of each flight path for each storm in storm-relative coordinates are included in Appendix A.

Once the data were placed in the storm-relative framework, the dropwindsonde winds in the lowest 150 m were extracted and averaged to define the WL150 wind (Franklin et al. 2003). Along with the average value of the WL150, the elevations of the top, bottom and midpoint of the layer were extracted. Also, the wind speed at the lowest reported dropwindsonde level was recorded. If the dropwindsonde did not provide a wind speed at a level of 10 m, it was not used. If the dropwindsonde did not record a wind speed and direction specifically at 10 m, a 10-m wind was interpolated from adjacent observations. All boundary layer wind data were recorded with and without storm motion. Using the dropwindsonde wind direction, tangential and radial winds of the TC were calculated from the u and v components.

The distributions of the locations of each WL150 wind speed and their co-located SFMR wind speeds for each radial leg flown through the three storms are contained in Appendix A. The radial distribution of flight-level wind speeds was used to determine the flight-level RMW and the location of each dropwindsonde was defined relative to the center of the storm. Then a relative radial distance from the storm center R* (Figure 13) was defined by dividing the radial distance between the dropwindsonde and TC center by the flight-level RMW. Therefore, if R* is less than one, the dropwindsonde was released inside the RMW. If the R* is one, the dropwindsonde was released at the RMW. Finally, if R* is greater than one, the dropwindsonde was released outside the RMW. The R* values were then used to categorize dropwindsondes based on their location relative to the flight-level RMW, except dropwindsondes with an R* of 10 or more were discarded as being too far from the storm center.

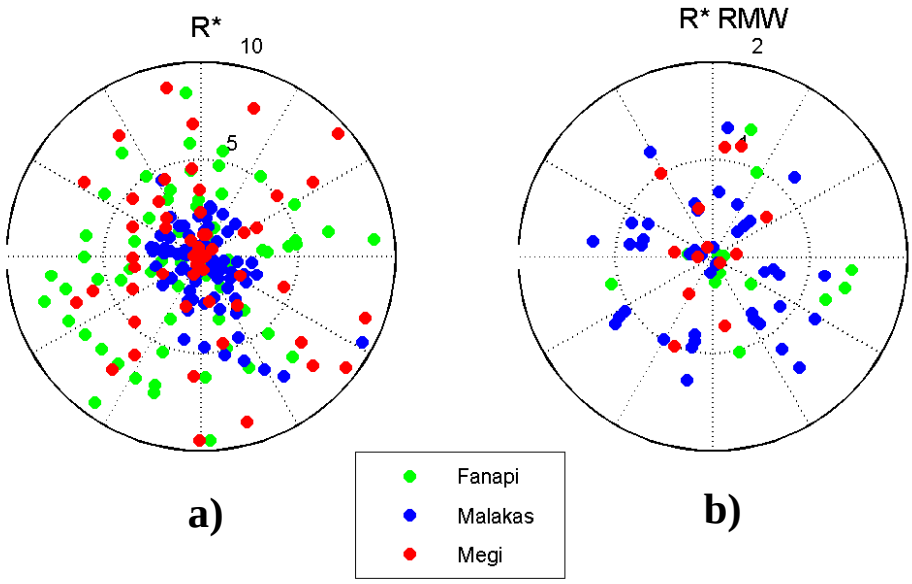

Figure 13. (a) Radial locations of all dropwindsondes from the three typhoons (color plots in inset) examined in this study. (b) The radial locations of all dropwindsondes with an R* value less than two. The dotted radius is the RMW and the solid radius is 2*RMW.

Several regression analyses will be performed to examine the linear relationships between various wind speed values: the WL150, 10-m interpolated wind speed, estimated surface wind speed, and SFMR wind speed estimates. The 10-m interpolated winds will be examined relative to SFMR winds, WL150 winds, and the Vsfc winds. The Franklin et al. (2003) eyewall-based surface adjustment method (Figure 11) will then be used to derive the surface wind speed based on the WL150.

Based on the R* values for each dropwindsonde, a first bin was specified for all of the dropwindsondes that were released inside the RMW. The second bin includes dropwindsondes that were within five km of the RMW. A third bin contains all dropwindsondes between the RMW and out to 3*RMW. A fourth bin contains

dropwindsondes between 3*RMW and 5*RMW. The fifth bin includes dropwindsondes beyond 5*RMW. For the second through fourth bins, a mean dropwindsonde wind profile was calculated at 5 min intervals each bin relative to the flight-level RMW. The vertical variations of wind speeds will be examined for each of these three bins. Finally, a normalized wind speed is defined as a ratio of the surface wind speed divided by the flight-level wind speed measured at approximately 700 hPa.

D. DATA SUMMARY

1. Typhoon Fanapi

The first typhoon observed in the ITOP experiment was TY Fanapi, which existed from 14 September 2010 to 18 September 2010. Of the six aircraft missions conducted into TY Fanapi, three were surveillance flights and three were reconnaissance flights. The three surveillance flights were not analyzed because they were conducted prior to the formation of TY Fanapi. Also, the square-spiral pattern of the surveillance flights does not provide for radial passes that are required to define the storm characteristics defined above. The SFMR data and dropwindsonde data from the three reconnaissance flights (Table 2) were analyzed to determine surface wind characteristics. During these flights, a total of 100 dropwindsondes were released from the WC-130J.

Table 2. Dropwindsondes available for analysis from three TY Fanapi WC-130J RECCO flights.

Flight	Mission Start	Mission End	Radial Legs	Dropwindsondes	Pattern
0420	1800 UTC Sep 15	0700 UTC Sep 16	4	25	Alpha
0520	1800 UTC Sep 16	0600 UTC Sep 17	4	23	Alpha
0620	1814 UTC Sep 17	0615 UTC Sep 18	6	52	Butterfly

Flight 0420 (Figures 27–28 in Appendix A-1) was flown as an alpha pattern into TS Fanapi. For flight 0520 (Figures 29–30 in Appendix A-1), a modified alpha pattern was flown. The final reconnaissance flight 0620 into Fanapi was on 17 September 2010

(Figures 31–33 in Appendix A-1). The flight pattern was a butterfly pattern that contained three center fixes with multiple dropwindsondes released in the center.

2. Typhoon Malakas

The second typhoon analyzed in the ITOP 2010 project was TY Malakas (Table 3), which became organized on 21 September 2010 and existed until 24 September 2010. During its life cycle, TY Malakas moved rapidly northward. Six flights were flown into TY Malakas by the ITOP WC-130J. A total of 94 dropwindsondes from the two reconnaissance flights into the mature TC were analyzed in this study. For flight 0322 (Figures 34–38 in Appendix A-2), a butterfly pattern was flown such that multiple center passes were available.

Table 3. Dropwindsondes available for analysis from two TY Malakas WC-130J RECCO flights.

Flight	Mission Start	Mission End	Radial Legs	Dropwindsondes	Pattern
0322	1413 UTC Sep 23	0101 UTC Sep 24	10	65	Butterfly
0422	1327 UTC Sep 24	0029 UTC Sept 25	4	29	Alpha

3. Typhoon Megi

Although TY Megi began to form on 13 October 2010, only two flights could be analyzed (Table 4) as they had patterns that allowed for the definition of the radial distribution of winds. A total of 76 dropwindsondes were released during the mature stages of TY Megi.

Table 4. Dropwindsondes available for analysis from two TY Megi WC-130J RECCO flights.

Flight	Mission Start	Mission End	Radial Legs	Dropwindsondes	Pattern
0430	1750 UTC Oct 14	0500 UTC Oct 15	6	32	Butterfly/ racetrack
0630	1815 UTC Oct 15	0600 UTC Oct 16	6	44	Butterfly

Flight 0430 (Figure 41–43 in Appendix A-3) into TS Megi had six radial legs that passed through the center of the storm. During an initial test of the dropwindsondes, a GPS reporting error was discovered that resulted in a loss of the first 200 hPa of data. This forced the aircraft to rise to a flight level of 12,000 feet for the remainder of the flight.

III. ANALYSIS

Increased understanding of the surface and boundary-layer winds of a mature TC will contribute to improved forecast accuracy of various oceanic and land impacts. Therefore, it is necessary to acquire and analyze *in-situ* observations obtained in the data-sparse regions over which TCs occur. This study compares *in-situ* aircraft observations and co-located dropwindsondes in three typhoons during ITOP 2010.

A. VERTICAL PROFILE CHARACTERISTICS OF TC

To analyze the vertical profiles of winds in a mature TC, the dropwindsonde data were categorized and averaged relative to the RMW at flight-level. The focus in this analysis is to identify radial variations in winds in the lowest layer of the storm in three regions (table 5): bin 2 (at the RMW), bin 3 (1 RMW beyond the RMW), and bin 4 (3 RMW from the center). Profiles were not plotted for dropwindsondes located in bin 1 and bin 5.

Table 5. Distribution of the dropwindsondes count based on their locations in relation to the RMW at flight level.

Bin number 1	R- RMW ≤ - 5 km	44 dropwindsondes
Bin number 2	-5 km ≤ R- RMW ≤ 5 km	22 dropwindsondes
Bin number 3	5 km < R- RMW < 3*RMW	91 dropwindsondes
Bin number 4	3*RMW ≤ R- RMW ≤ 5*RMW	31 dropwindsondes
Bin number 5	R- RMW ≥ 5*RMW	91 dropwindsondes

1. Average Vertical Wind Profiles

For each bin, the averaged vertical profile of total wind speed (Figure 14a) is nearly above a surface layer in which the wind varies as a near log-linear profile (not shown). The wind speed vertical profile at the RMW increases rapidly just below the flight level, which is at an average level of 2850 m. Below 2300 m, the wind speed

profile only increases gradually to the maximum wind value below 500 m. Therefore, it appears that the majority of the dropwindsondes in this category were dropped just inside the flight-level RMW, and then descended into the sloping eyewall and higher wind speeds.

The level of maximum winds varies relative to the location of the RMW. For the sondes beyond three times the RMW, the maximum wind is located near 900 m. In the region between the RMW and two times the RMW from the storm center, the maximum winds occur at 600 m. Near the RMW, the level of maximum winds has decreased to 200 m.

The vertical profiles of wind speeds normalized by the wind speed at flight-level (Figure 14b) has similar characteristics as for the vertical profiles actual wind speed. Beyond the RMW, the ratio of surface winds to flight-level wind is approximately 0.8, which is similar to the ratio defined by Franklin et al. (2003). At the RMW, the ratio of surface winds to flight-level winds is 1.2, which is much larger than any ratio defined by Franklin et al. (2003) or Powell et al. (2009). This may be due to the data from TY Megi, which was a very intense and small typhoon, and this will be investigated by examining each storm individually.

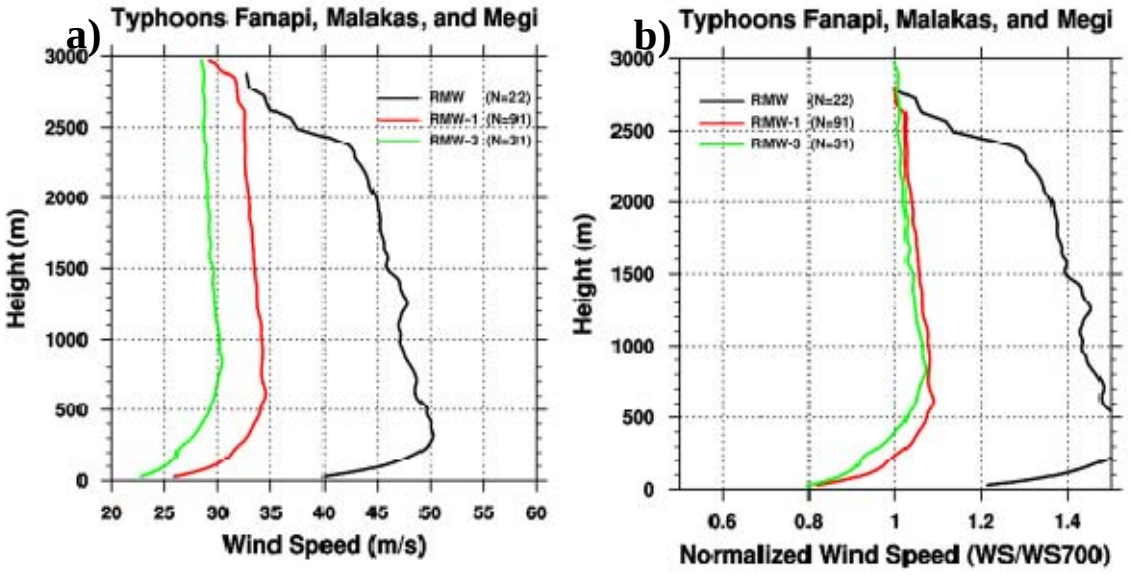

Figure 14. (a) Averaged vertical profiles of actual wind speeds (m s^{-1}) from all dropwindsondes in three ITOP storms. (b) Averaged vertical profiles of wind speeds normalized by wind speeds at flight-level for the individual dropwindsondes. The line definitions in terms of the RMW are given in the inset.

2. Typhoon Fanapi Profiles

The averaged vertical profile of actual wind speed for TY Fanapi (Figure 15a) for the outer two bins have almost constant wind speeds from just below flight level to the level of maximum winds. The averaged wind speed profile for the winds near the RMW increases gradually from flight-level to the maximum wind at approximately 300 m above the surface. This averaged profile of winds near the RMW suggests that the dropwindsondes in TY Fanapi were released just inside the flight-level RMW, and the eyewall slope was gradual as the measured wind speeds generally increased as the sonde descended.

The level of maximum winds in TY Fanapi decreases in altitude relative to the location of the RMW. For sondes released at locations more than three times the RMW, the maximum wind is at approximately 800 m. In the region between the RMW and two times the RMW from the center of the storm, the maximum winds occur at 500 m. Near the RMW, the level of maximum winds has decreased to 300 m.

The normalized wind speed vertical profiles at regions beyond the RMW for TY Fanapi (Figure 15b) also have a mean constant wind speed from flight-level down to near the level of maximum winds. The ratio of flight-level wind speeds to surface wind speeds outside of the RMW is 0.85, which is similar to the ratio calculated by Franklin et al. (2003). The ratio of flight-level to surface winds from dropwindsondes near the RMW is near 1.0, which is also consistent with Franklin et al. (2003).

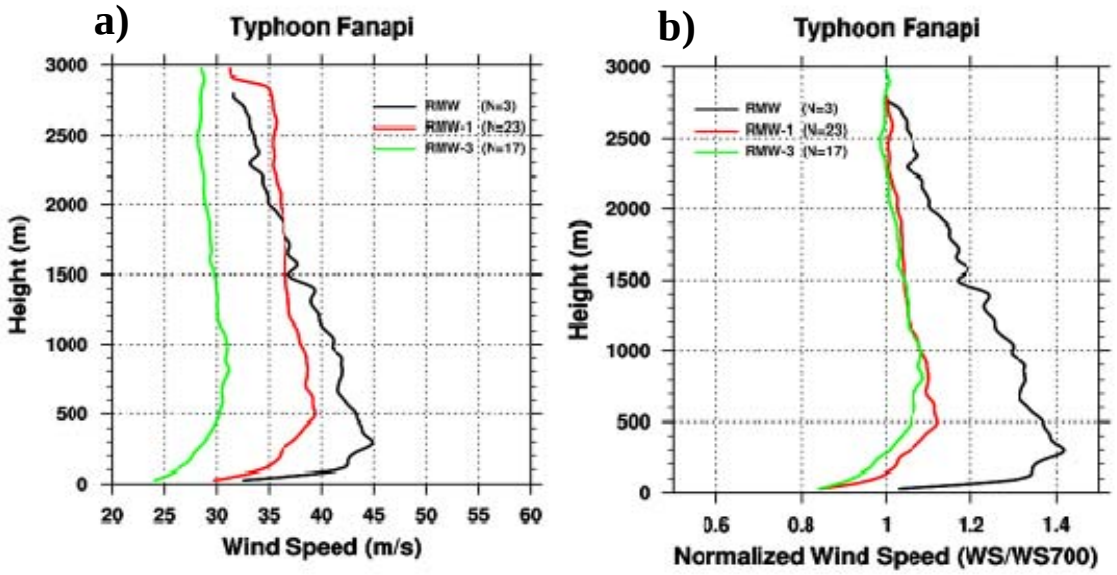

Figure 15. (a) Averaged vertical profiles of actual wind speed (m s^{-1}) as in Figure 14a, except only for TY Fanapi. (b) Averaged vertical profiles of wind speeds normalized by the wind speed at flight-level winds for TY Fanapi.

3. Typhoon Malakas Profiles

The averaged vertical profile of actual wind speeds for TY Malakas (Figure 16a) also has almost constant wind speeds above the level of maximum winds. The averaged wind speed profile near the RMW increases only slightly from flight-level to the RMW, which is located at 400 m. The slight variation in the vertical profile of wind speeds above the level of maximum winds for the RMW bin suggests that the eyewall had a very

small slope. This is consistent with the radial profile of flight-level winds and SFMR winds (Figures 34–40 Appendix A-2) that indicate that the inner region of Malakas was very broad with large asymmetry.

For Malakas, the level of maximum wind is higher in the region three times the RMW than the region just outside the RMW. This wind structure is a possible result of the larger number of dropwindsondes averaged in the outer storm bin. This larger number of dropwindsondes could have resulted in a smooth profile. For the outer region, the height of the maximum wind speeds is 900 m. For the inner region the level of maximum winds is at 600 m. The height of the maximum winds in the RMW bin is 400 m.

The vertical profile of winds normalized by the wind speed at flight-level (Figure 16b) has similar characteristics to the actual wind speed vertical profile. However, there is one slight difference in the outer two profiles. In the normalized profile, the ratio of flight-level winds to surface winds in the bin that is three times the RMW is slightly smaller than the same ratio for the bin two times the RMW. This is different from the profiles of the actual wind but it is what is expected. These ratios are near 0.8, which is similar to the ratio calculated by Franklin et al. (2003). For the dropwindsondes near the RMW, the ratio is 1.0.

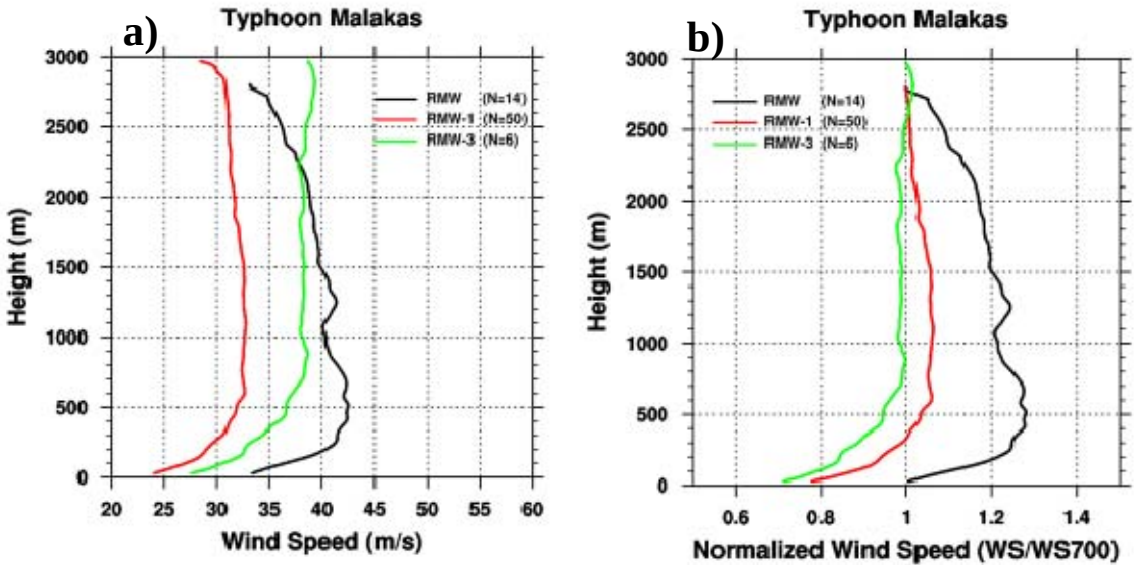

Figure 16. (a) Averaged vertical profiles of actual wind speed (m s^{-1}) as in Figure 14a, except only for TY Malakas. (b) Averaged vertical profiles of winds normalized by the values of the flight-level wind for TY Malakas.

4. Typhoon Megi Profiles

The averaged vertical profile of actual wind speeds for TY Megi (Figure 17a) for each bin has a near constant wind speed from flight-level down to the surface layer. The outer two regions of this storm have similar profiles with maximum winds located at the same height near 700 m. For the profile of dropwindsondes released near the RMW, the wind speeds are almost double the speed of the winds in the outer regions of the storm. In addition to the large wind speeds, the vertical profile for the RMW has similar characteristics as in Fanapi and Malakas as wind speeds gradually increase until the level of maximum wind is reached at 300 m. As found with the other storms, the level of maximum winds decreases in height as the radial distance to the center of the storm decreases.

A difference between TY Megi and the other two typhoons is that the normalized vertical profile of wind speeds (Figure 17b) near the RMW has a near constant value above the level of maximum winds. Therefore, the slope of the eyewall of TY Megi was small, which would be expected for such a small, intense storm. The ratio of flight-level

winds to surface winds over the two outer regions of the storm is 0.8, which is consistent with Franklin et al. (2003). The ratio of flight-level to surface winds is 1.0 for the dropwindsondes in the RMW bin.

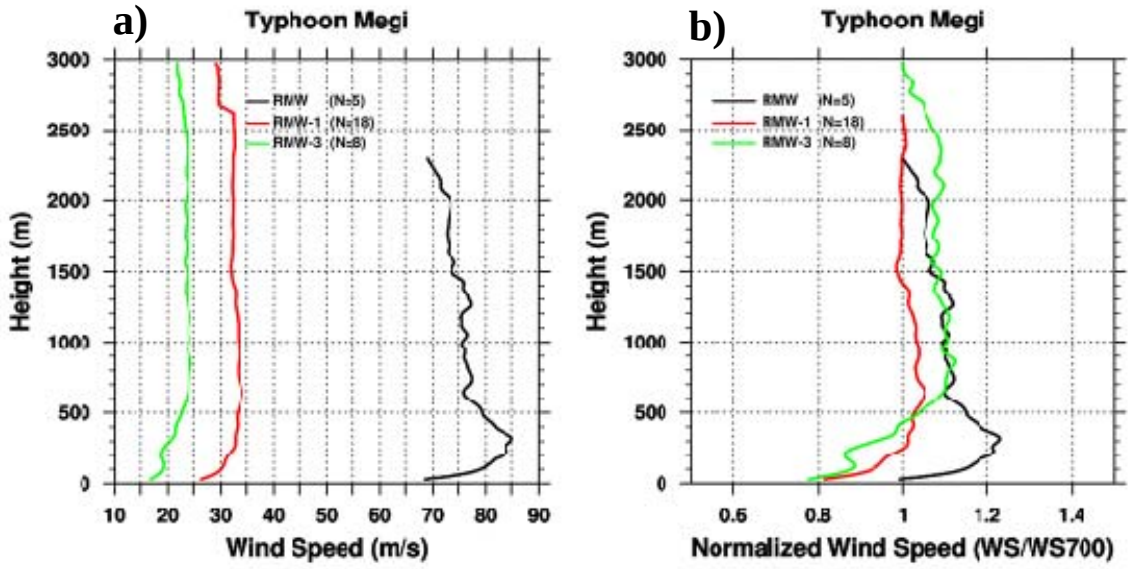

Figure 17. (a) Averaged vertical profiles of wind speed (m s^{-1}) as in Figure 14a, except only for TY Megi. (b) Averaged vertical profiles of winds normalized by the values of the flight-level wind for TY Megi.

5. Summary

The vertical profiles of the winds for the three ITOP 2010 storms portray variability and commonality in general structure of these TCs. TY Fanapi had a relatively steep sloping eyewall and a decrease in winds outwards from the center of the storm. The structure of TY Malakas was less organized with the stronger winds in the outer edges of the storm than near the RMW. Finally, the structure of STY Megi was a very intense but compact storm with a large change in wind speeds from the eyewall to the outer edge of the storm. The vertical profile of wind speeds on the RMW of Megi were near constant above the level of maximum winds, which indicated that there is little slope to the eyewall.

B. SURFACE WIND FIELD

As indicated above, various estimates of surface winds are defined from the GPS dropwindsonde, SFMR, and flight-level data. Using observations from the WC-130J SFMR and GPS dropwindsondes, a data set of boundary layer winds has been defined. This data set includes wind speeds at the lowest level reported by the dropwindsonde, the WL150, 10-m interpolated wind, and the SFMR-estimated surface wind speed. These wind speeds were created for each of the seven flights discussed above.

Four comparisons of low-level wind measurements have been performed via linear least-square regressions. The WL150 wind speed was compared to the 10-m interpolated wind speed, the calculated surface wind speed (Vsfc) was compared to the 10-m interpolated wind speed, and the 10-m interpolated wind speed was compared to the SFMR surface wind speeds. These four comparisons were chosen to examine the relationships between the one-minute surface averaged winds and the SFMR calculated wind speeds as defined by the flow diagram in Figure 18. For each comparison, six regressions were calculated. The first regression includes all wind speeds in the data set, and then regressions were separately calculated for the dropwindsondes in each of the five categories relative to the RMW (Table 5). The summary of these regression calculations is provided in Table 6.

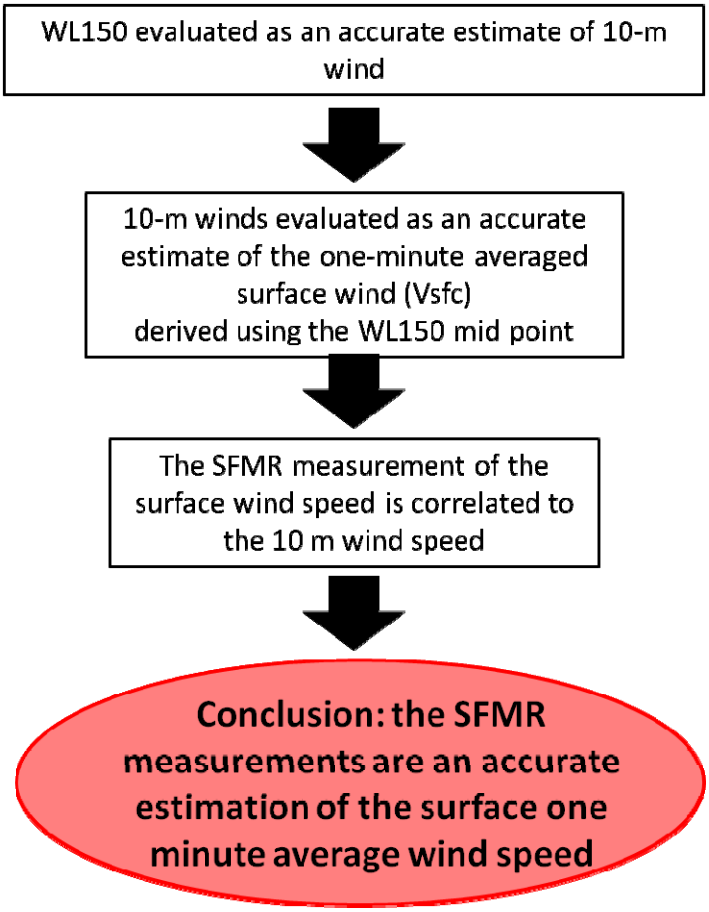

Figure 18. Flow chart that defines the progression of statistical regression analyses for the relationship among estimates of one-minute average surface wind speeds.

Table 6. Summary of the regression statistics in terms of explained variance (R^2) for the regressions outlined in Figure 18 for all data and the five bins defined in Table 5.

	WL150 vs. 10m		**Vsfc vs. 10m**		**10m vs. SFMR**	
Bin number	# of obs	R^2	# of obs	R^2	# of obs	R^2
All Data	167	.9468	165	.9207	136	.7968
1	32	.96	32	.9591	32	.8603
2	12	.7923	12	.815	12	.744
3	71	.8886	67	.7946	64	.5209
4	27	.927	27	.9449	21	.5886
5	73	.8895	73	.8685	64	.6164

Regression analyses comparing WL150 and 10-m winds for all bins are presented in this section. For the remaining regression analyses, only the results for the combined data set are presented in subsequent sections. Regression analyses for the individual bins are provided in Appendix B.

1. WL150 Winds vs. 10-m Winds

The WL150, which is the average wind speed over the lowest 150 m for each dropwindsonde, is proposed to be an estimate of the 10-m wind. If a dropwindsonde did not report winds down to a level of 10 m, then no comparison with the WL150 could be made. If no wind speed was reported specifically at the 10 m level, then a value at 10 m was interpolated from adjacent values. The slope of the regression line of 10-m winds relative to the WL150 is 0.85 and 95 percent of the variability in the 10-m wind is explained by this relationship with the WL150. These regression results are consistent with the analysis of Uhlhorn et al. (2007), who analyzed several Atlantic TCs from the 2005 season and also found a line slope of 0.85. A slight slow bias in the 10-m wind when regressed upon the WL150 wind speed occurs for wind speeds above 40 m s^{-1} (Figure 19).

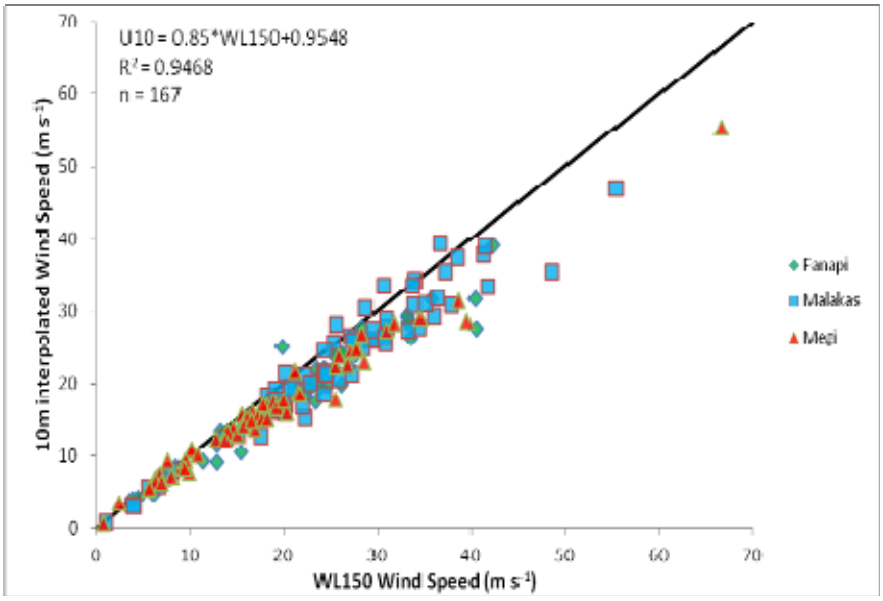

Figure 19. Scatter plot of 10-m interpolated wind speeds and WL150 wind speeds for the entire data set from three typhoons (see insert for color code) during ITOP 2010.

a. Bin Number One

There were 32 dropwindsondes released that were more than 5 km and inside the RMW (i.e., Bin 1), and reported wind speeds that extended below 10 m (Table 6). For this subset, a close fit to the regression line is found with r-squared equal to 0.96 (Figure 20). The unusual large WL150 wind speeds in this Bin are all from TY Malakas. These large winds are attributed to the special structure of Malakas, which had a rather broad inner core and large wind asymmetry (Figures 34–40 Appendix A-2).

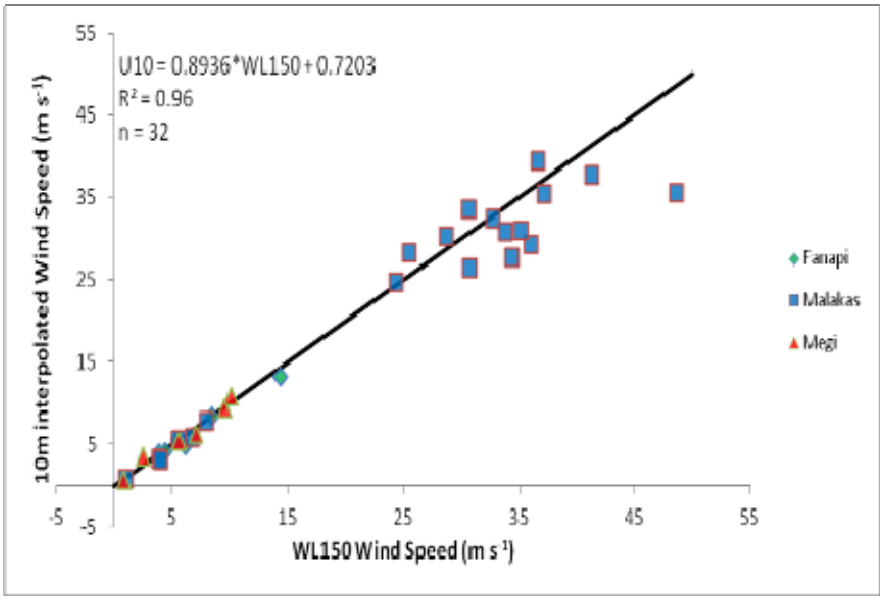

Figure 20. Scatter plot of 10-m interpolated wind speeds and WL150 wind speeds as in Figure 19, except for the Bin 1 category of dropwindsondes released more than 5 km inside the RMW.

b. Bin Number Two

There were 12 dropwindsondes deployed within 5 km of the RMW that reported winds below 10 m (Figure 21). For this Bin 2 data set, the r-squared value is 0.7923 (Table 6). The smaller slope for this regression is attributed to the large number of values from Malakas and Fanapi. The small r-squared value is attributed to the WL150 regression line leading to an underestimate of the 10-m wind in the core of STY Megi.

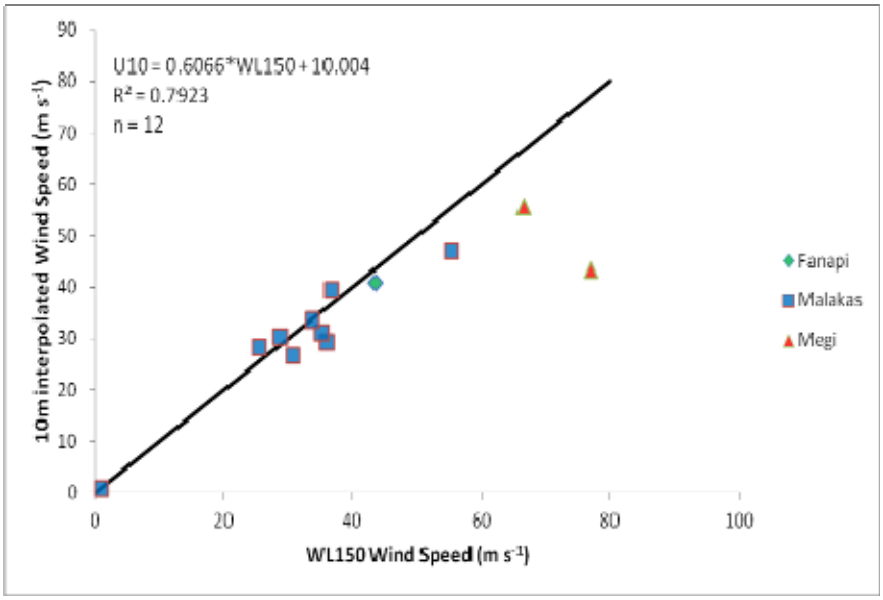

Figure 21. Scatter plot of 10-m interpolated wind speeds and WL150 wind speeds as in figure 19, except for the Bin 2 dropwindsondes released near the RMW.

c. Bin Number Three

There were 71 drops between the RMW and a radius of three times the RMW (Figure 22). Although this regression resulted in an r-squared value of 0.8886 (Table 6), at wind speeds greater than 15 m s^{-1} there is a low bias in the 10-m interpolated winds for all three storms. The slope being less than one also indicates a slight low bias in the estimation of the 10-m wind for the WL150.

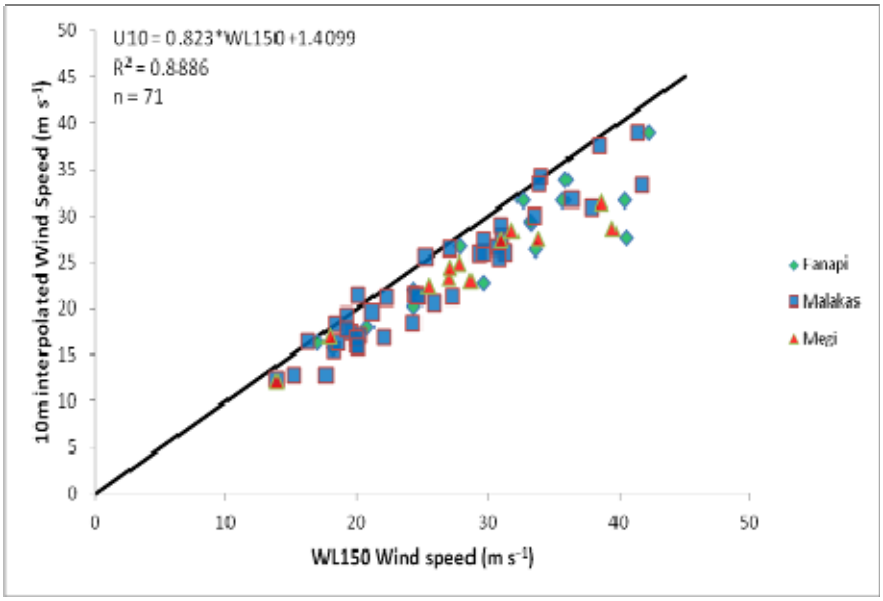

Figure 22. Scatter plot of 10-m interpolated wind speeds and WL150 wind speeds as in Figure 19, except for the Bin 3 dropwindsondes released in the region between the RMW and three times the RMW.

d. Bin Number Four

There are 27 dropwindsondes in the region between three times the RMW and five times the RMW from the TC center that had wind speed values below 10 m (Figure 23). As in the other bins the slope of the regression line is slightly less than 1.0. Although the r-squared value for this regression is 0.927 (Table 6), there is a slight low bias with respect to the estimate of the 10-m wind from the WL150 wind speeds.

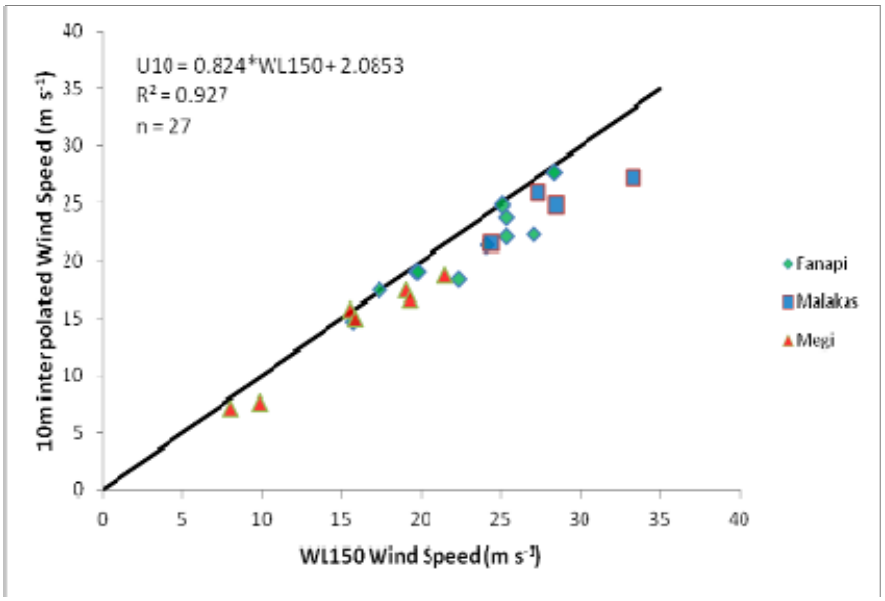

Figure 23. Scatter plot of 10-m interpolated wind speeds and WL150 wind speeds as in Figure 19, except for the Bin 4 dropwindsondes released in the region between three times the RMW and five times the RMW.

e. Bin Number Five

There were 73 dropwindsondes released beyond five times the RMW from the center that reported wind speeds less than 10 m. The wind speed regression has an r-squared value of 0.8895 (Table 6). In this case, the slope of the regression line is larger than 1.0 (Figure 24). However, there is a tendency for the 10-m wind to be less than the WL150 wind for speeds larger than 20 m s^{-1}.

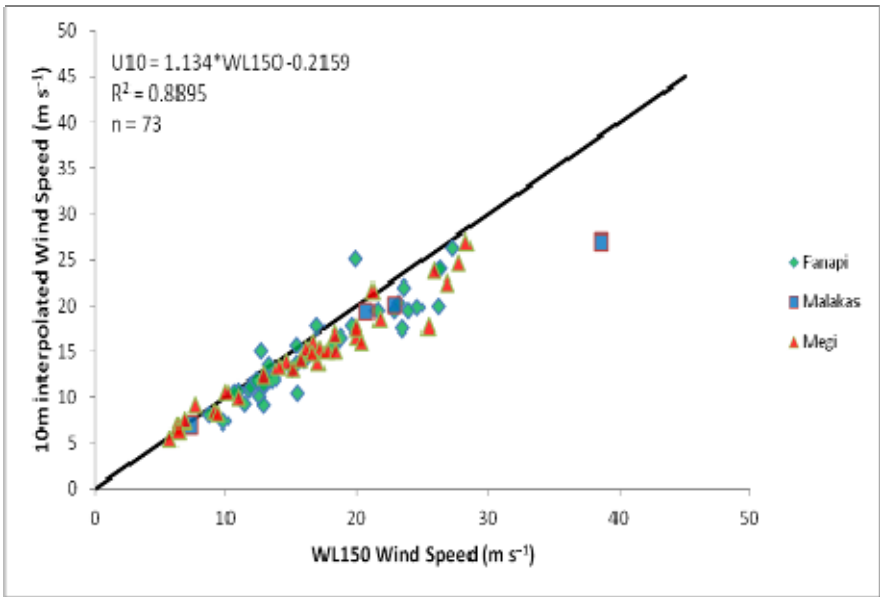

Figure 24. Scatter plot of 10-m interpolated wind speeds and WL150 wind speeds as in Figure 19, except for the Bin 5 dropwindsondes released beyond five times the RMW.

2. Vsfc Winds vs. 10-m Winds

The method of Franklin et al. (2003) was used to estimate the surface wind speed from the WL150. Franklin et al. (2003) used the WL150 mid-point height with an empirically derived dropwindsonde-based mean eyewall profile to calculate the ratio of the surface wind speed to the WL150. This ratio was then multiplied by the WL150 wind speeds for all flights to estimate a surface wind speed Vsfc. This value was then regressed upon the 10-m interpolated wind speed, which resulted in a regression slope of 0.92 (Figure 25). Uhlhorn et al. (2007) found a slope of 1.02 for the same two variables for data from Atlantic TCs.

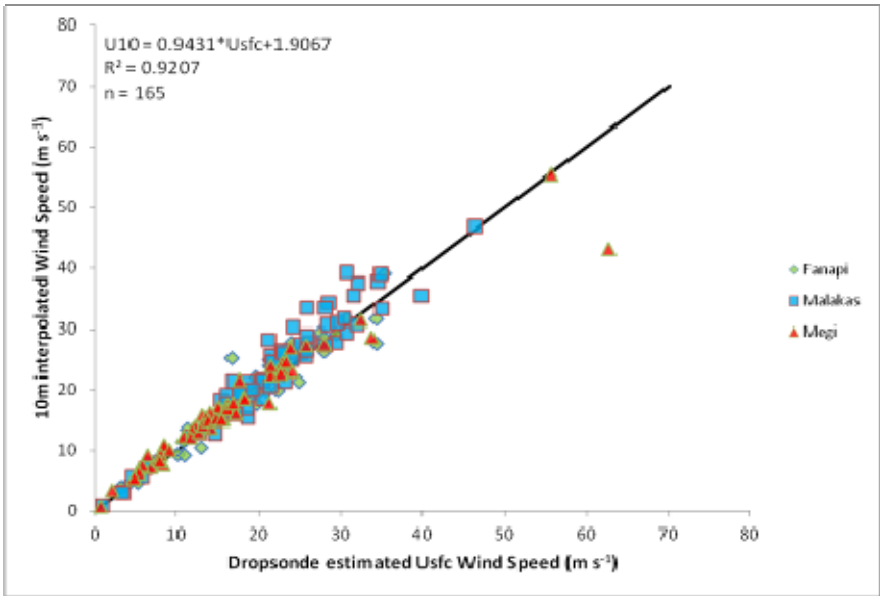

Figure 25. Scatter plot of 10-m interpolated wind speeds and Vsfc wind speeds for the entire set of winds from the three ITOP 2010 typhoons.

Although this method of estimation for surface winds was based on a mean eyewall wind profile, it appears to be valid for dropwindsondes near the RMW as well as beyond the RMW (Figures 47–51 in Appendix B). The accuracy of this mean eyewall wind profile outside of the eye was also noticed by Uhlhorn et al. (2007) from their 2005 sample of Atlantic TCs. The r-squared values for Bins 3–5 outside the RMW are slightly smaller than the r-squared values for the all-data sample in Figure 25 (Figures 49–51).

3. 10-m Winds vs. SFMR Winds

The final comparison was between the SFMR and the 10-m interpolated wind from the dropwindsondes, which is taken as an estimate of the one-minute average surface wind. For the all-data sample the regression line slope is 1.02 (Figure 26). The analysis of 10-m winds and SFMR wind by Uhlhorn and Black (2003) resulted in a regression slope of 0.98. Therefore, the results for the ITOP cases are similar to those of the large set of Atlantic cases examined by Uhlhorn and Black (2003). Again, the high wind speed SFMR values for TY Megi deviate well to the right of the regression line, which may be due to the compact structure of Megi. Significant departures from the regression line also occur for wind speeds below 10 m s^{-1}.

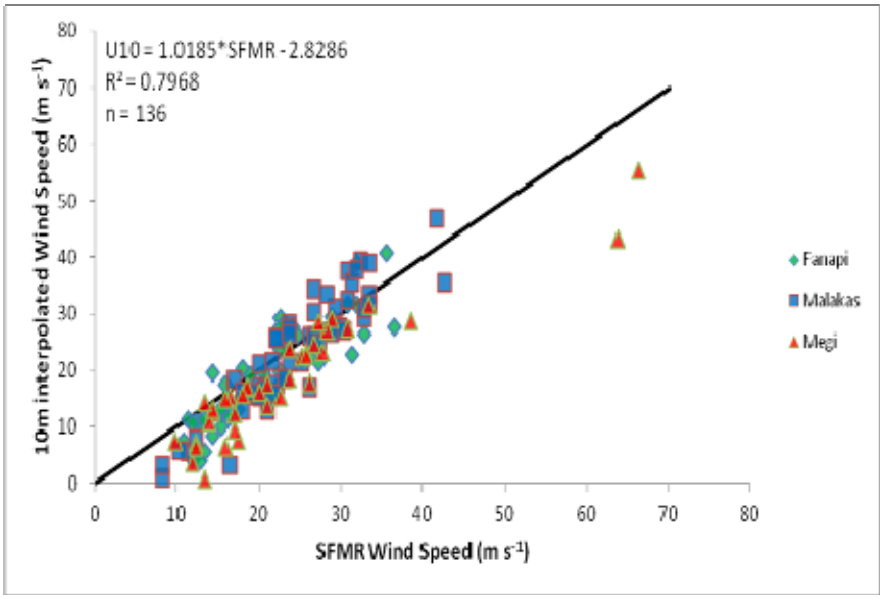

Figure 26. Scatter plot of 10-m interpolated wind speeds and SFMR wind speeds for the entire set of winds from the three ITOP 2010 typhoons.

For the regressions based on data in individual bins (Figures 52–56 in Appendix B), the r-squared values are near 0.6 in the region beyond three times the RMW (Figures 55 and 56). This relationship in r-squared appears to be due to an increased variability in SFMR-based surface winds, which is likely due to the varying structural characteristics of the ITOP storms.

4. Summary

The comparison of the WL150 winds and 10-m winds indicates a significant relationship exists between the two measures that may be used to represent a surface-averaged one-minute wind. Also, the comparison between the 10-m winds and the SFMR winds indicates a significant relationship exists between the remotely sensed wind speeds and the measured 10-m wind speeds. Consequently, the SFMR is a good representation of the one-minute average surface wind speed.

The results of these comparisons and the similarity to relationships from the samples of Atlantic TCs indicate that similar wind estimation methods apply in both basins. The variations among the regression results for the five bins relative to the RMW indicate the regression results are less significant farther from the RMW. For the comparisons of the 10-m winds with the Vsfc estimation, the reduction in significance is attributed to the extrapolation method that was designed to be used in the eyewall. For the other comparisons, the reduction in significance away from the TC center may be due to the small sample sizes and the variety of storm structures among Fanapi, Malakas, and Megi.

IV. CONCLUDING REMARKS

A. SUMMARY

Tropical cyclones are intense phenomena that can cause immense damage to populated areas. As a result of increasing population in the TC impacted regions, it is necessary to understand as much about these weather phenomena as possible. Through an in-depth analysis of *in-situ* data, it is possible to increase understanding of structure and intensity changes of TCs. Data sets obtained in large field programs over the WPAC is a potential for improving knowledge of TCs applicable to both the Atlantic and the Pacific basins.

This study used data from the ITOP 2010 field experiment to analyze the surface wind characteristics in three mature TCs. Data were obtained using the U.S. Air Force 53rd Weather Reconnaissance Squadron WC-130J aircraft. This dataset included GPS dropwindsonde profile information, flight-level weather data, and SFMR surface estimated wind speeds and rain rates. Several surface wind parameters were calculated: 10-m interpolated wind speeds, WL150 wind speeds, and the wind speeds at the lowest dropwindsonde reported level. These surface wind parameters were calculated for seven reconnaissance flights into three typhoons during ITOP 2010. A total of 270 GPS dropwindsondes from these seven flights were used along with approximately 84 hours of flight level and SFMR data.

Comparisons between the SFMR and 10-m interpolated winds were calculated to determine the application of these tools to estimate surface winds in the WPAC. It was found that SFMR estimates and the 10-m interpolated wind speeds were well correlated. Also a significant linear relationship was documented between the 10-m winds and derived surface winds. Although advances in the SFMR surface wind estimates have been made over the past few years (Uhlhorn et al. 2007), a bias was documented at both smaller and larger wind speeds.

To further the study of the surface wind field in TCs, the location of each dropwindsonde was defined relative to the flight-level RMW. For all wind comparisons,

the regression significance decreased for regions farther away from the RMW, which is attributed to variations in storm structure among the three typhoons. It is anticipated that an increase in sample size would improve the significance in the outer storm regimes. Nevertheless, these statistical regression results indicate that the remotely sensed SFMR surface wind measurements are accurate and consistent within a range of wind speeds between 10 m s^{-1} to 55 m s^{-1}. Outside this range some bias exists.

The three typhoons investigated during ITOP have different structural characteristics as defined in the average vertical profiles of winds and the radial distribution of winds for each flight (see Appendix A). Even with the structural variation, the distribution of winds used for the regression analyses are well mixed, meaning that the general distribution of wind speeds is similar for all storms.

The results of this thesis agree well with findings from other studies completed for the Atlantic basin, and support the results from TCS-08 described by Havel (2009) and Heck (2011). Therefore, it is hoped that increased use of the ITOP-2010 data observations will lead to improved understanding of TC structure over the WPAC. With improvements in the ability for track and intensity forecasting, better preparations for these intense weather phenomena will mitigate property damage and minimize loss of life.

B. RECOMMENDATIONS

This thesis focused on the analysis of the surface wind speed characteristics inside mature TCs. In this study, the bins were defined by dropwindsonde release positions relative to the flight-level RMW. It would be interesting to condition the data based on storm intensity, motion, and size, but this will require a larger sample of storms. Analysis of the wind directional changes in the boundary layer of mature TCs can yield important information about the impacts on the ocean. While an initial attempt was made to define the inflow angle for each dropwindsonde, the results were inconsistent due to the relatively small sample size in each bin. These results obtained from this aircraft reconnaissance data set indicate the importance of *in-situ* data observations inside these

typhoons to enhance knowledge of surface wind characteristics. Therefore, more *in-situ* data measurement missions should be completed in the WPAC.

THIS PAGE INTENTIONALLY LEFT BLANK

APPENDIX A. RADIAL LEG CROSS-SECTIONS

1. FANAPI

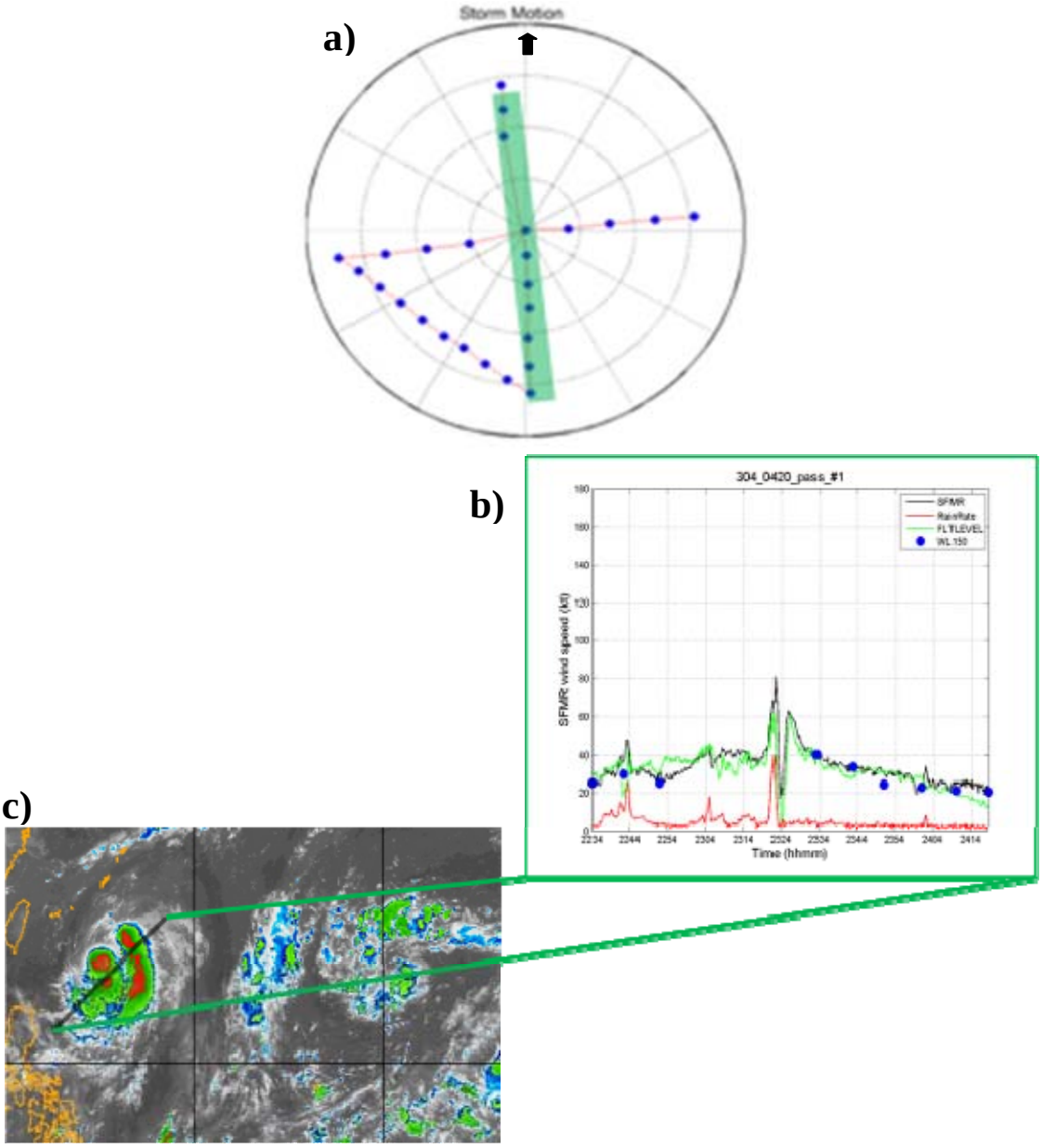

Figure 27. a) Storm-relative motion flight track for flight 0420 in TY Fanapi with aircraft pass number one highlighted in green. b) Cross-section of SFMR and flight-level wind speeds for Fanapi flight 0420 pass number one. The WL150 wind speeds calculated for each dropwindsonde in the pass are defined by the blue circles. c) Enhanced infrared geostationary satellite image at the central time of flight 0420. Pass number one is defined by the black line.

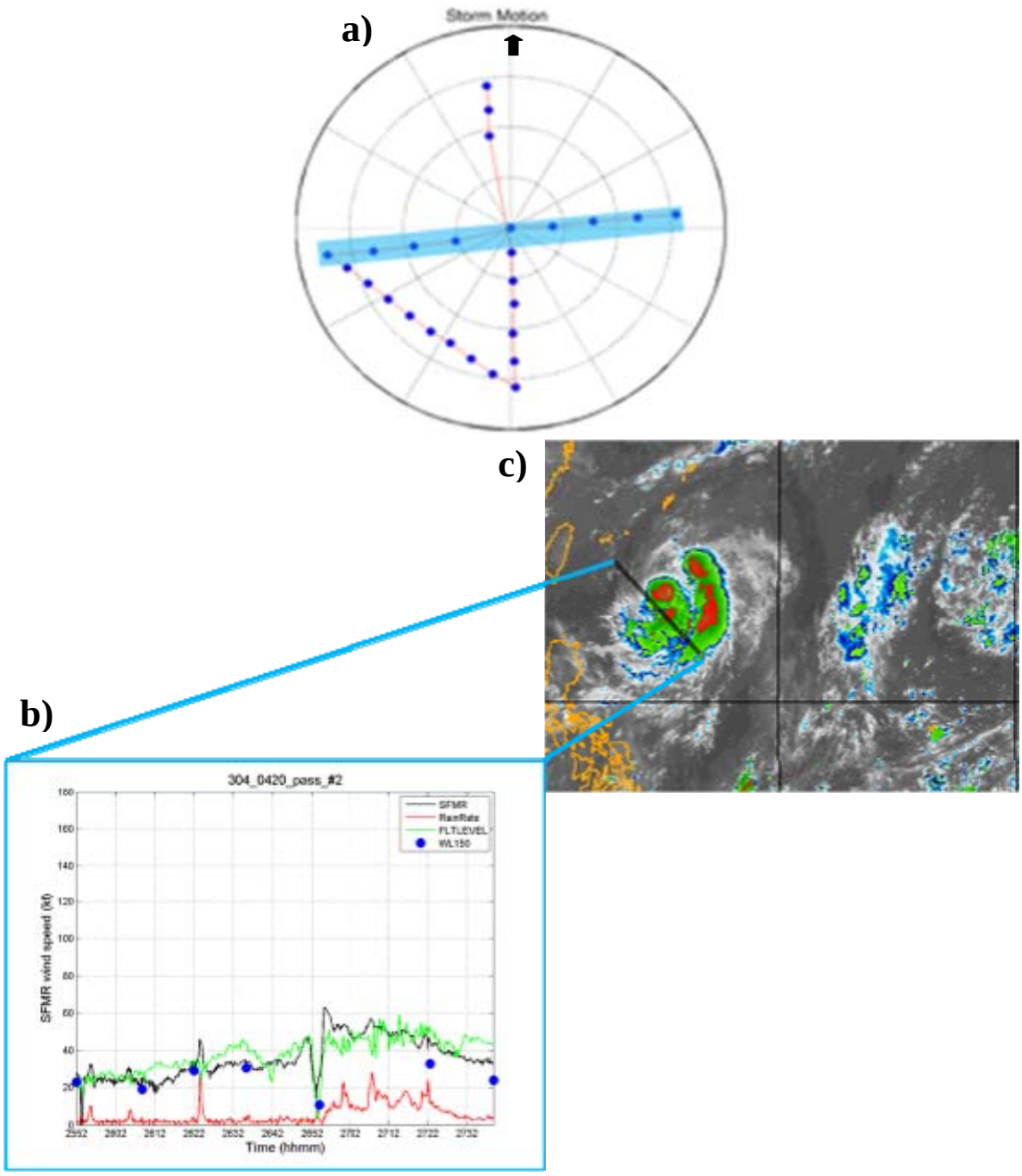

Figure 28. a) Storm-relative motion flight track for flight 0420 in TY Fanapi with aircraft pass number two highlighted in blue. b) Cross-section of SFMR and flight-level wind speeds for Fanapi flight 0420 pass number two. The WL150 wind speeds calculated for each dropwindsonde in the pass are defined by the blue circles. c) Enhanced infrared geostationary satellite image at the central time of flight 0420. Pass number two is defined by the black line.

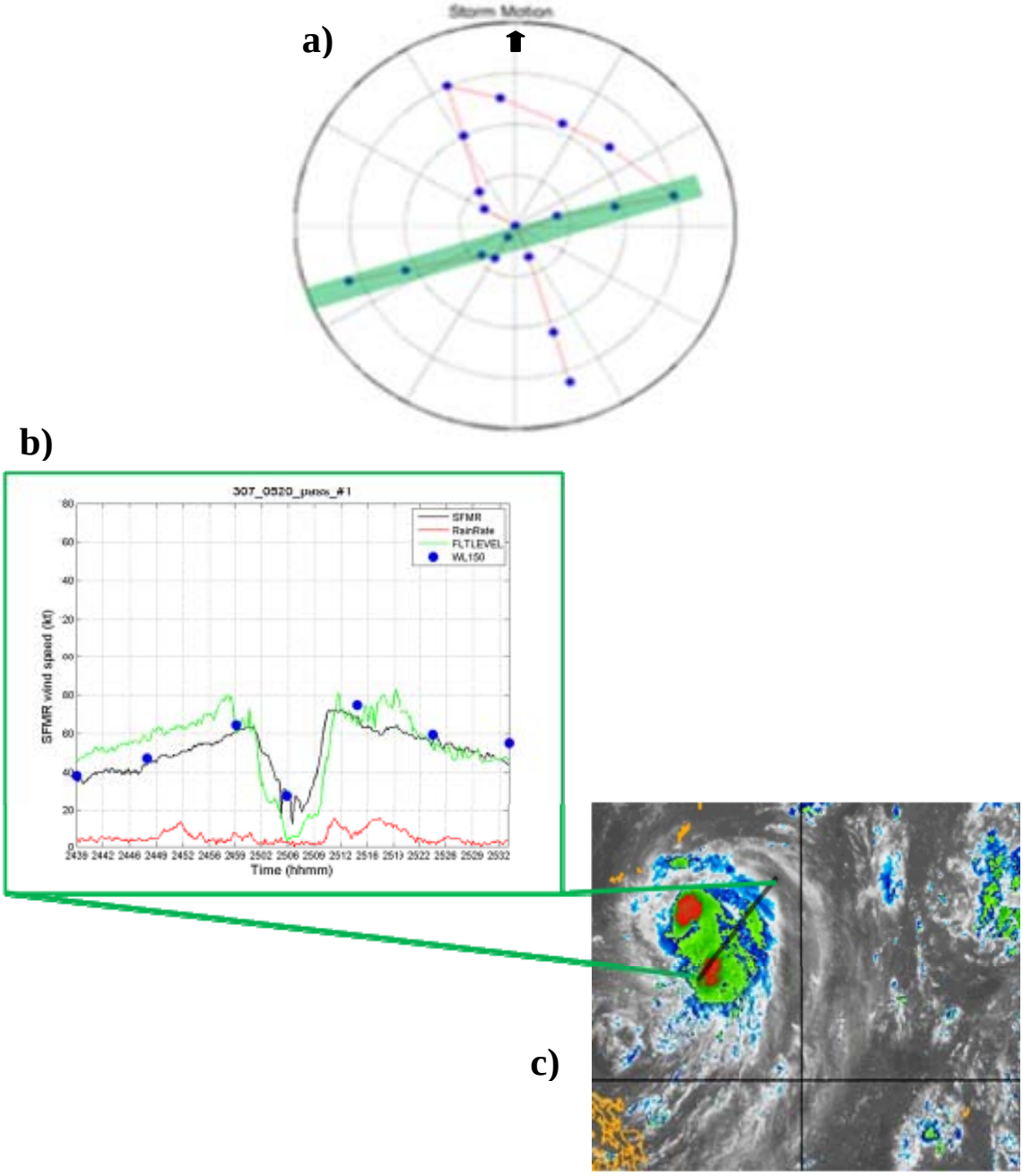

Figure 29. a) Storm-relative motion flight track for flight 0520 in TY Fanapi with aircraft pass number one highlighted in green. b) Cross-section of SFMR and flight-level wind speeds for Fanapi flight 0520 pass number one. The WL150 wind speeds calculated for each dropwindsonde in the pass are defined by the blue circles. c) Enhanced infrared geostationary satellite image at the central time of flight 0520. Pass number one is defined by the black line.

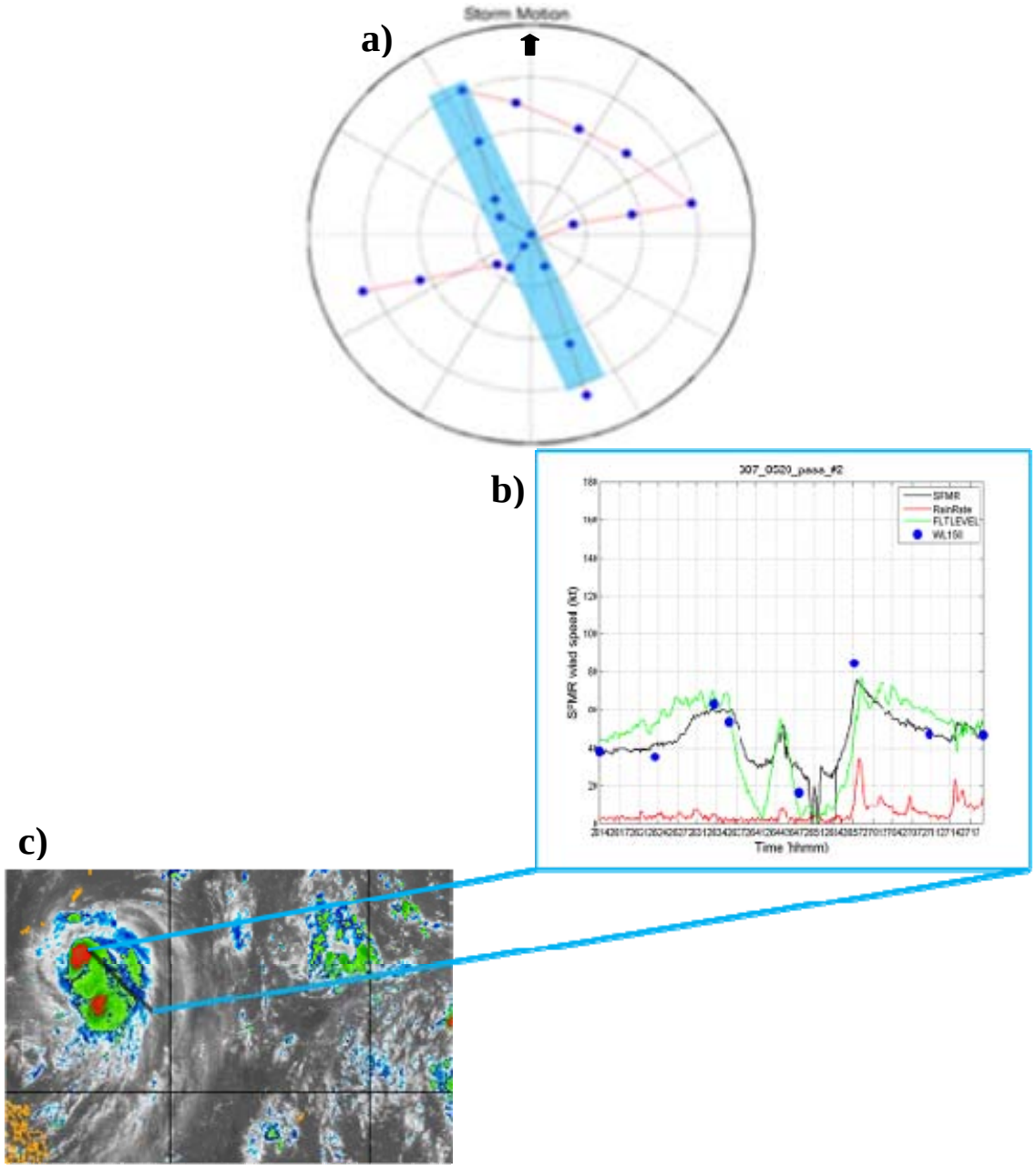

Figure 30. a) Storm-relative motion flight track for flight 0520 in TY Fanapi with aircraft pass number two highlighted in blue. b) Cross-section of SFMR and flight-level wind speeds for Fanapi flight 0520 pass number two. The WL150 wind speeds calculated for each dropwindsonde in the pass are defined by the blue circles. c) Enhanced infrared geostationary satellite image at the central time of flight 0520. Pass number two is defined by the black line.

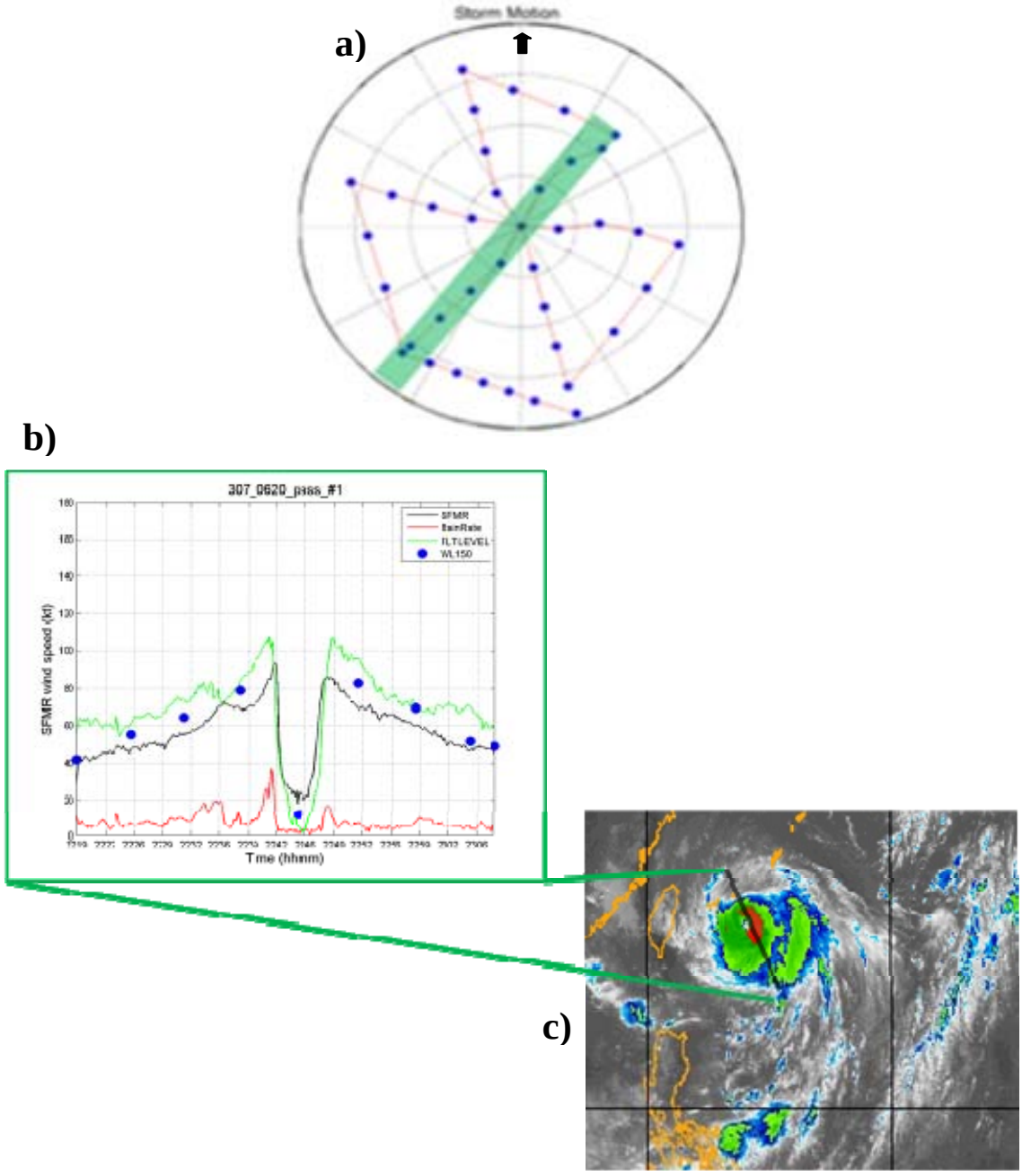

Figure 31. a) Storm-relative motion flight track for flight 0620 in TY Fanapi with aircraft pass number one highlighted in green. b) Cross-section of SFMR and flight-level wind speeds for Fanapi flight 0620 pass number one. The WL150 wind speeds calculated for each dropwindsonde in the pass are defined by the blue circles. c) Enhanced infrared geostationary satellite image at the central time of flight 0620. Pass number one is defined by the black line.

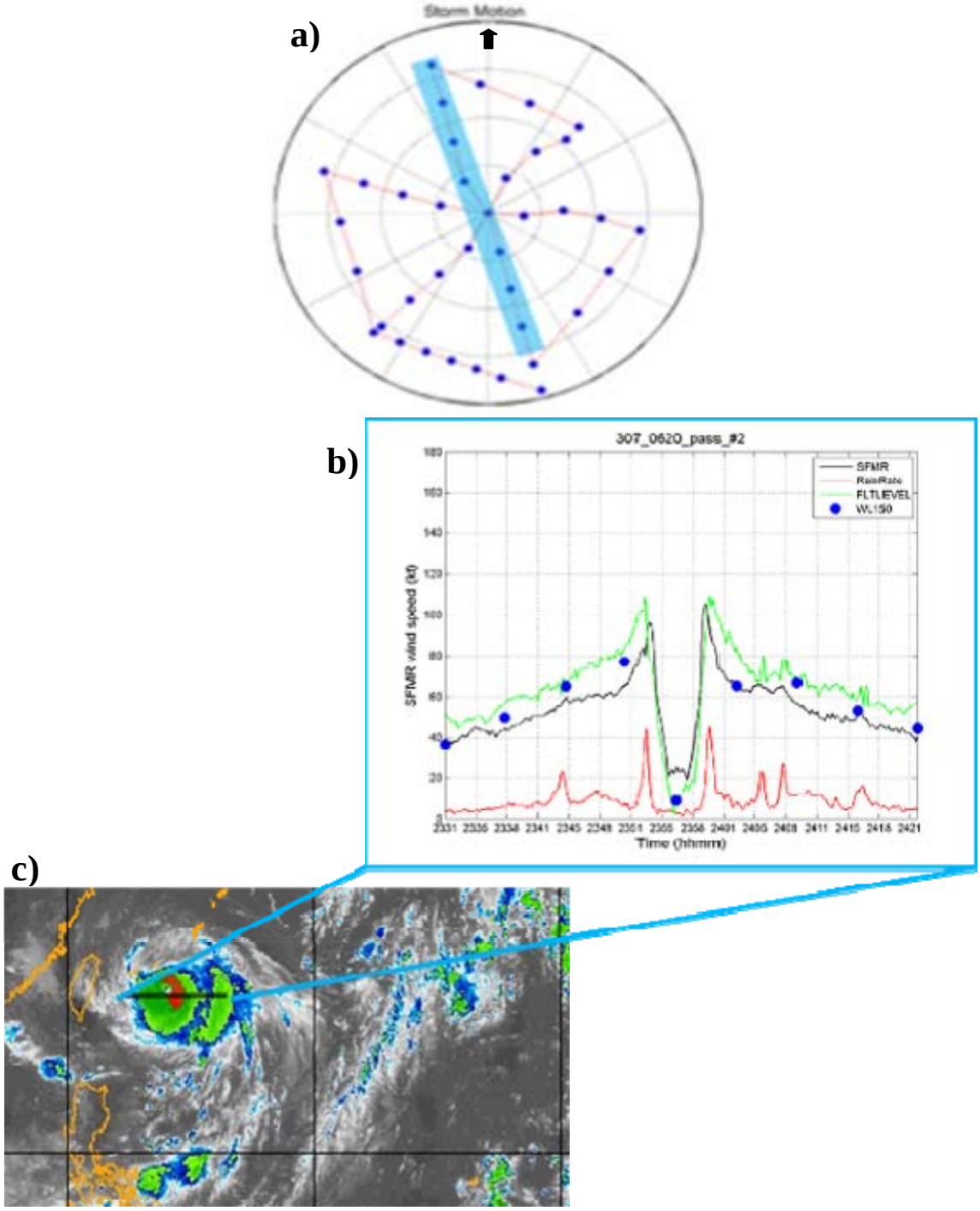

Figure 32. a) Storm-relative motion flight track for flight 0620 in TY Fanapi with aircraft pass number two highlighted in blue. b) Cross-section of SFMR and flight-level wind speeds for Fanapi flight 0620 pass number two. The WL150 wind speeds calculated for each dropwindsonde in the pass are defined by the blue circles. c) Enhanced infrared geostationary satellite image at the central time of flight 0620. Pass number two is defined by the black line.

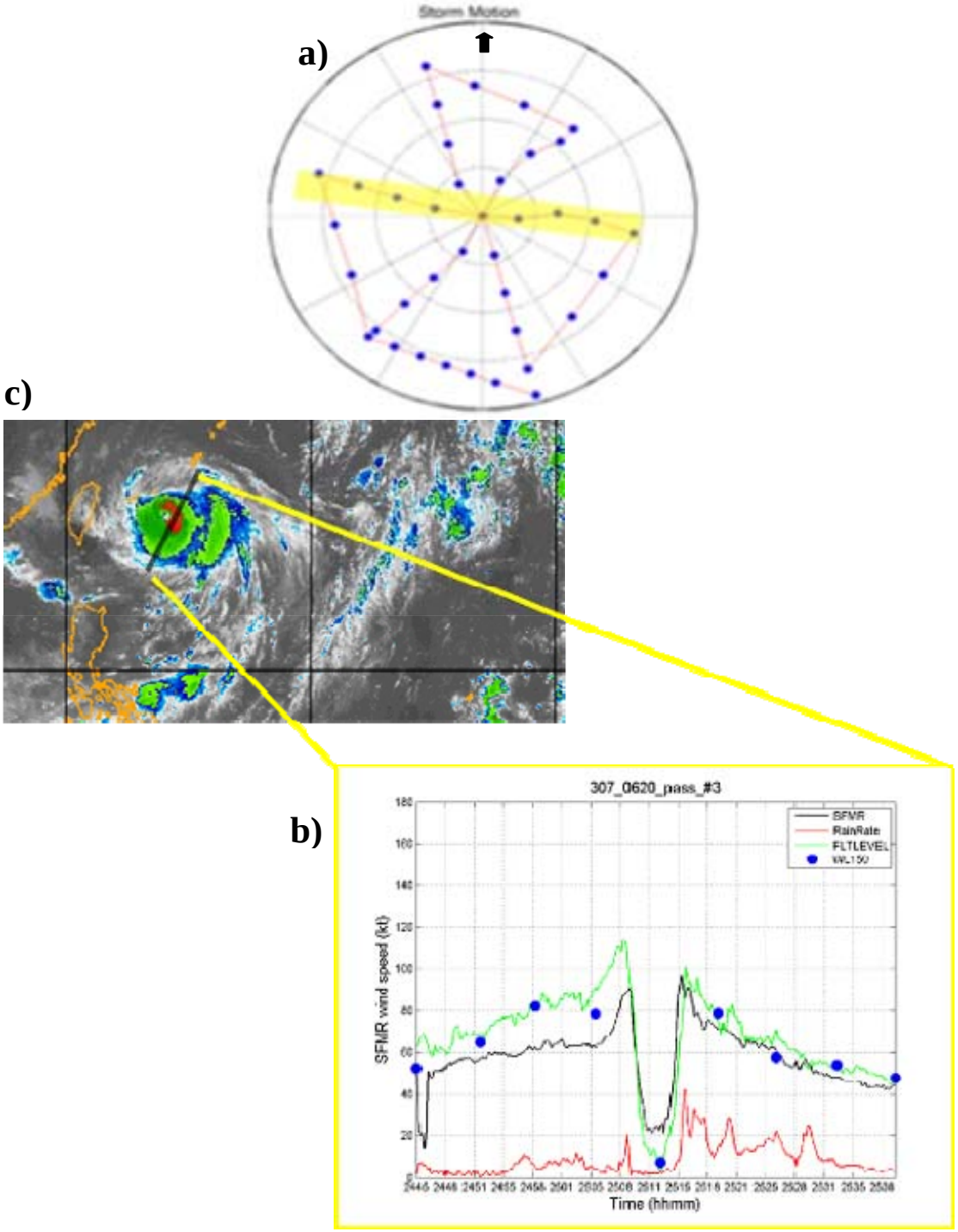

Figure 33. a) Storm-relative motion flight track for flight 0620 in TY Fanapi with aircraft pass number three highlighted in yellow. b) Cross-section of SFMR and flight-level wind speeds for Fanapi flight 0620 pass number three. The WL150 wind speeds calculated for each dropwindsonde in the pass are defined by the blue circles. c) Enhanced infrared geostationary satellite image at the central time of flight 0620. Pass number three is defined by the black line.

2. MALAKAS

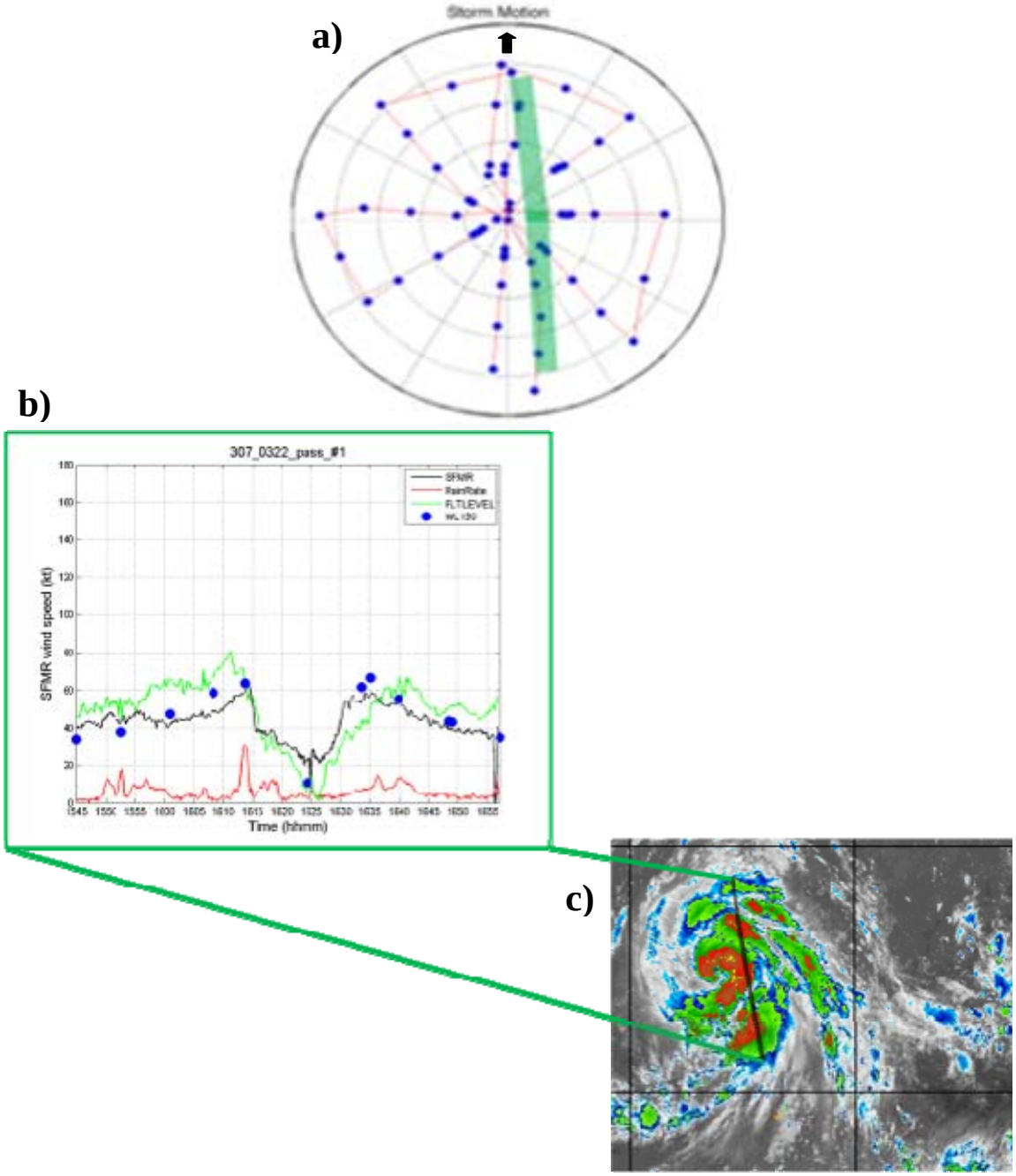

Figure 34. a) Storm-relative motion flight track for flight 0322 in TY Malakas with aircraft pass number one highlighted in green. b) Cross-section of SFMR and flight-level wind speeds for Malakas flight 0322 pass number one. The WL150 wind speeds calculated for each dropwindsonde in the pass are defined by the blue circles. c) Enhanced infrared geostationary satellite image at the central time of flight 0322. Pass number one is defined by the black line.

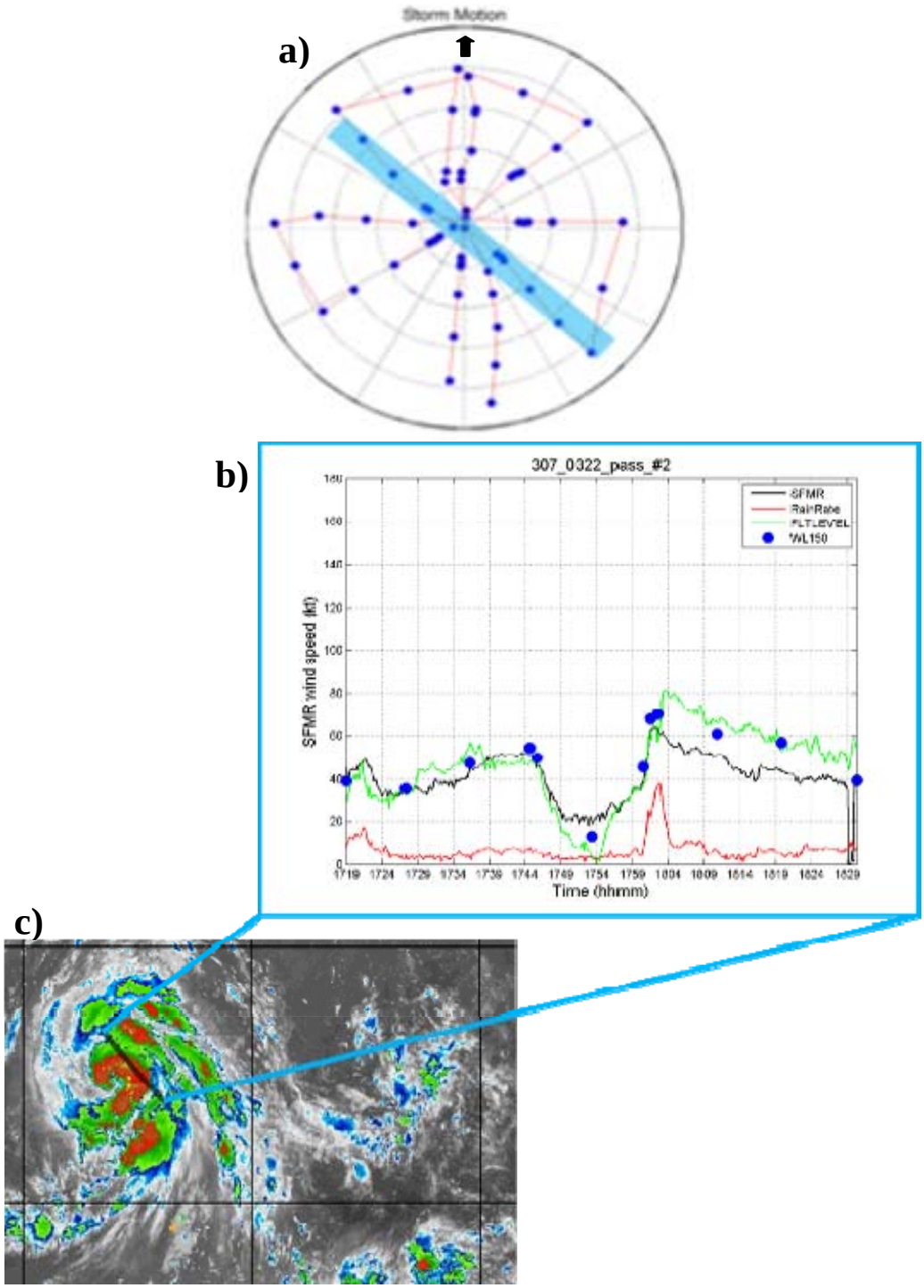

Figure 35. a) Storm-relative motion flight track for flight 0322 in TY Malakas with aircraft pass number two highlighted in blue. b) Cross-section of SFMR and flight-level wind speeds for Malakas flight 0322 pass number two. The WL150 wind speeds calculated for each dropwindsonde in the pass are defined by the blue circles. c) Enhanced infrared geostationary satellite image at the central time of flight 0322. Pass number two is defined by the black line.

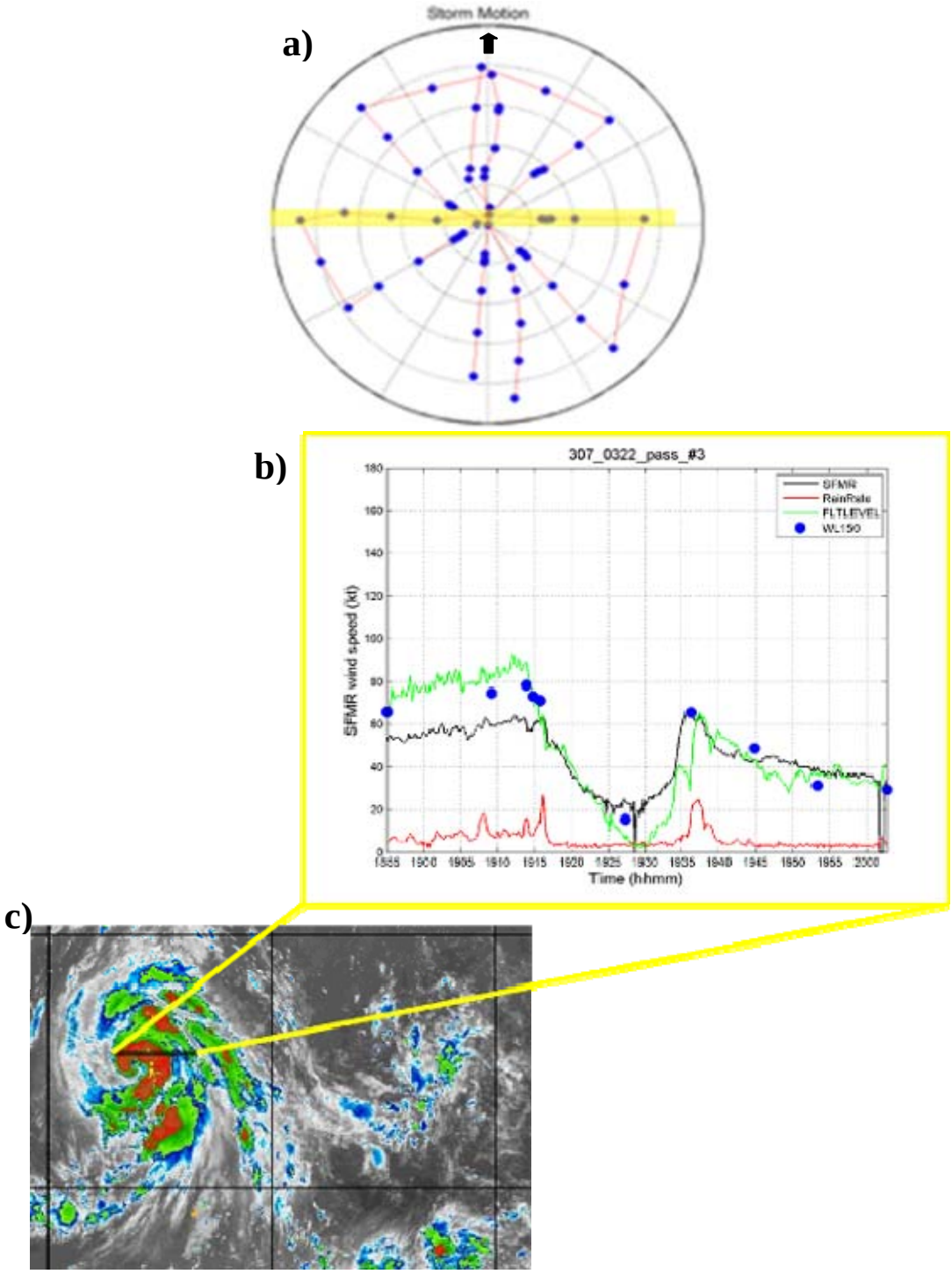

Figure 36. a) Storm-relative motion flight track for flight 0322 in TY Malakas with aircraft pass number three highlighted in yellow. b) Cross-section of SFMR and flight-level wind speeds for Malakas flight 0322 pass number three. The WL150 wind speeds calculated for each dropwindsonde in the pass are defined by the blue circles. c) Enhanced infrared geostationary satellite image at the central time of flight 0322. Pass number three is defined by the black line.

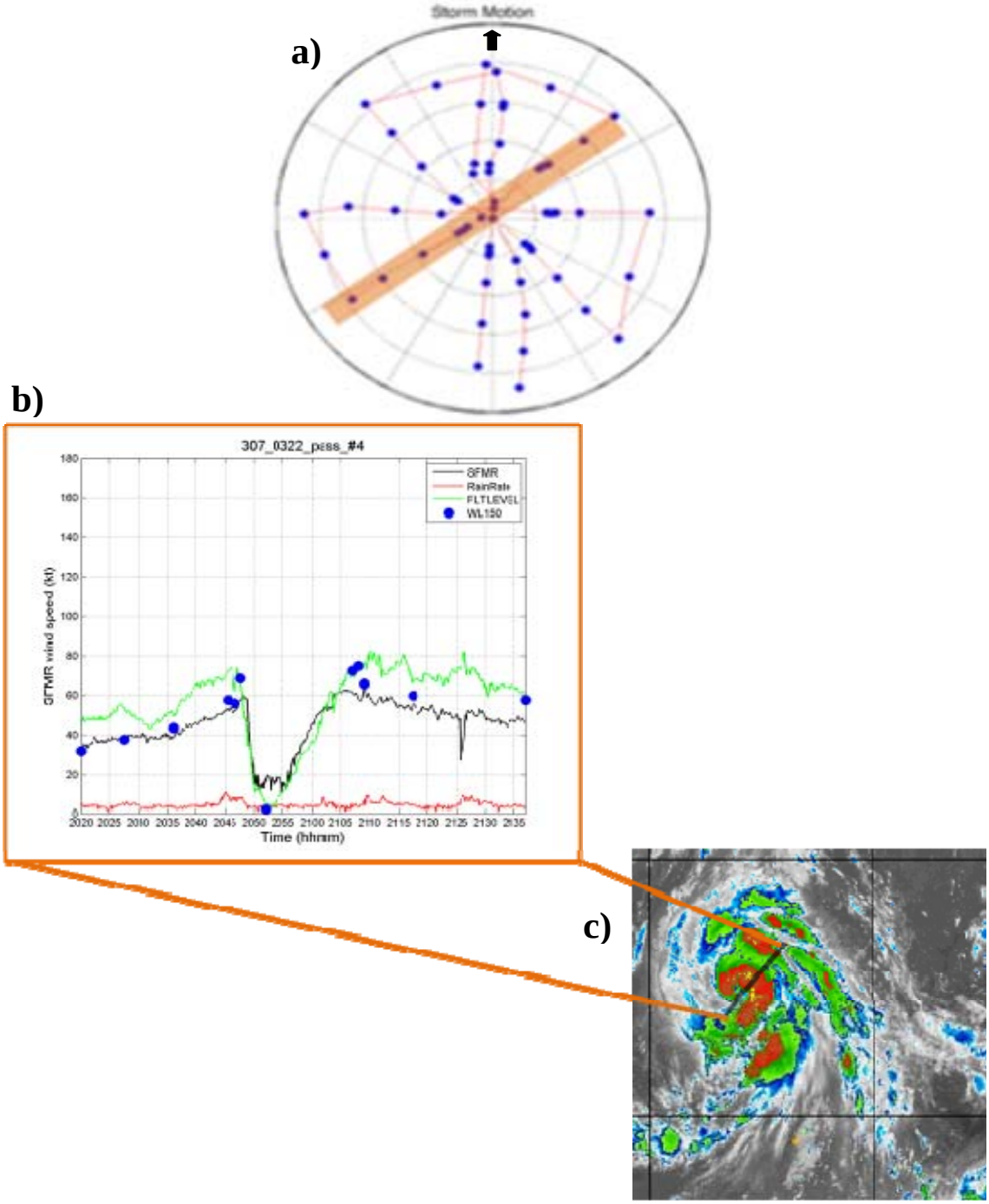

Figure 37. a) Storm-relative motion flight track for flight 0322 in TY Malakas with aircraft pass number four highlighted in orange. b) Cross-section of SFMR and flight-level wind speeds for Malakas flight 0322 pass number four. The WL150 wind speeds calculated for each dropwindsonde in the pass are defined by the blue circles. c) Enhanced infrared geostationary satellite image at the central time of flight 0322. Pass number four is defined by the black line.

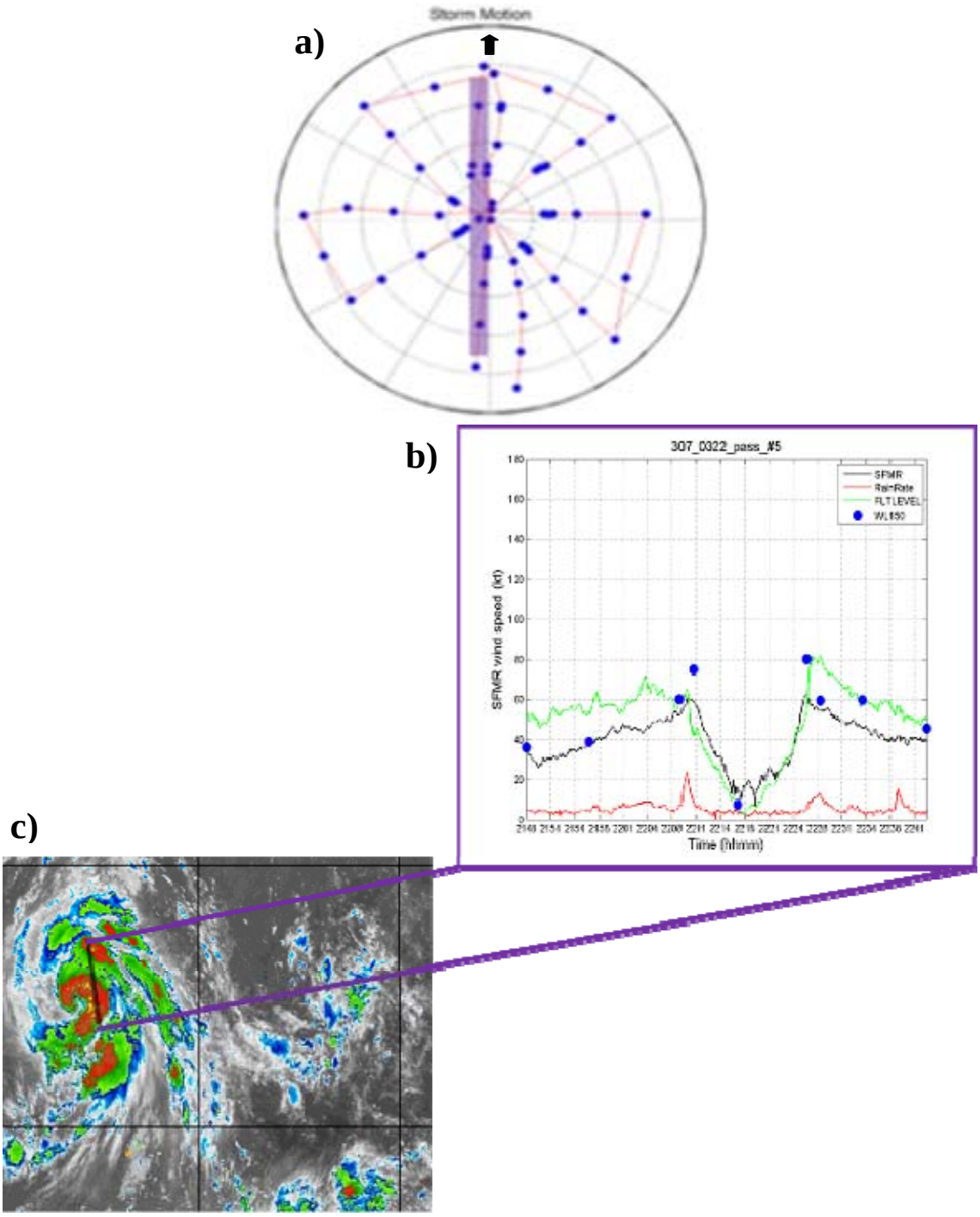

Figure 38. a) Storm-relative motion flight track for flight 0322 in TY Malakas with aircraft pass number five highlighted in purple. b) Cross-section of SFMR and flight-level wind speeds for Malakas flight 0322 pass number five. The WL150 wind speeds calculated for each dropwindsonde in the pass are defined by the blue circles. c) Enhanced infrared geostationary satellite image at the central time of flight 0322. Pass number five is defined by the black line.

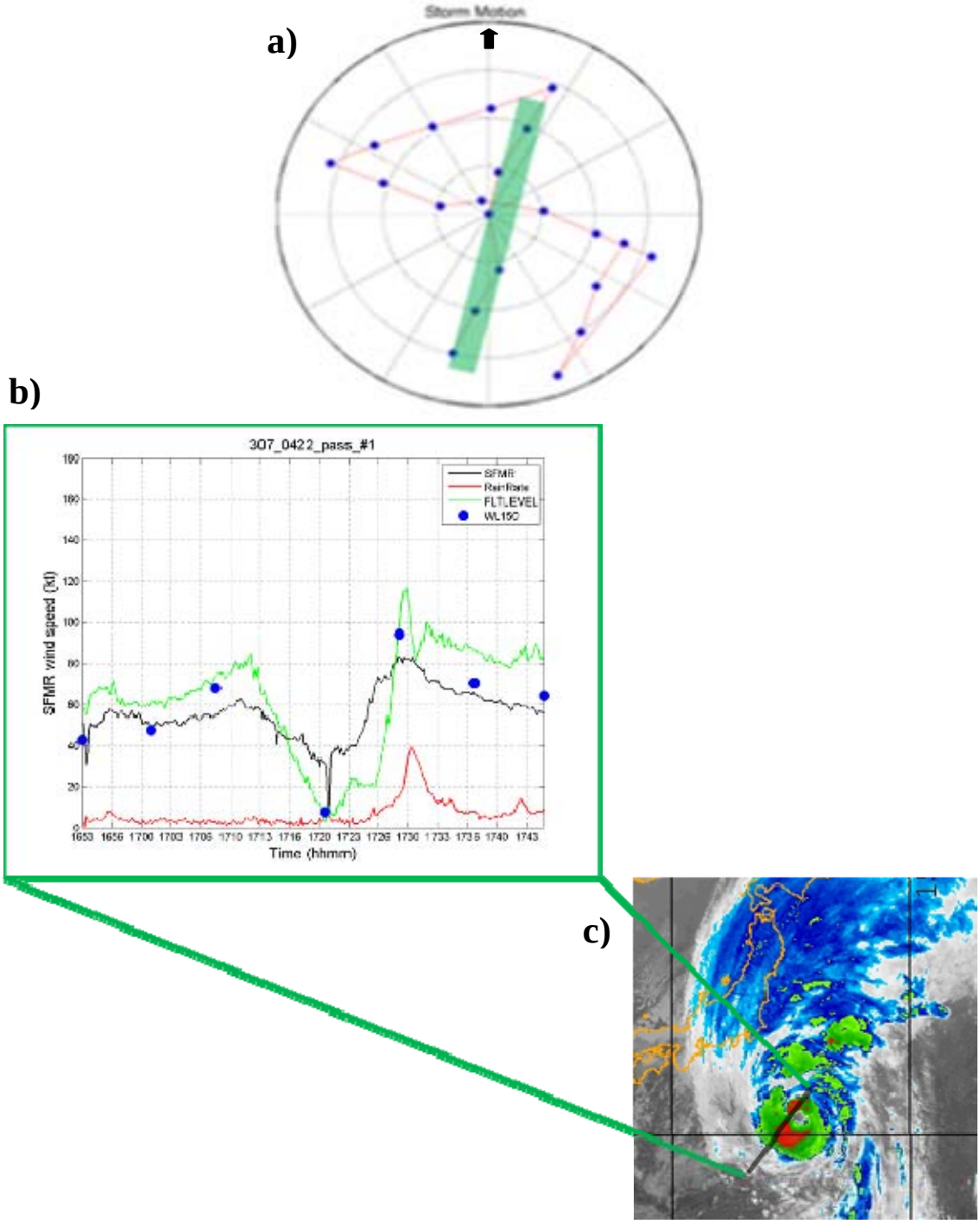

Figure 39. a) Storm-relative motion flight track for flight 0422 in TY Malakas with aircraft pass number one highlighted in green. b) Cross-section of SFMR and flight-level wind speeds for Malakas flight 0422 pass number one. The WL150 wind speeds calculated for each dropwindsonde in the pass are defined by the blue circles. c) Enhanced infrared geostationary satellite image at the central time of flight 0422. Pass number one is defined by the black line.

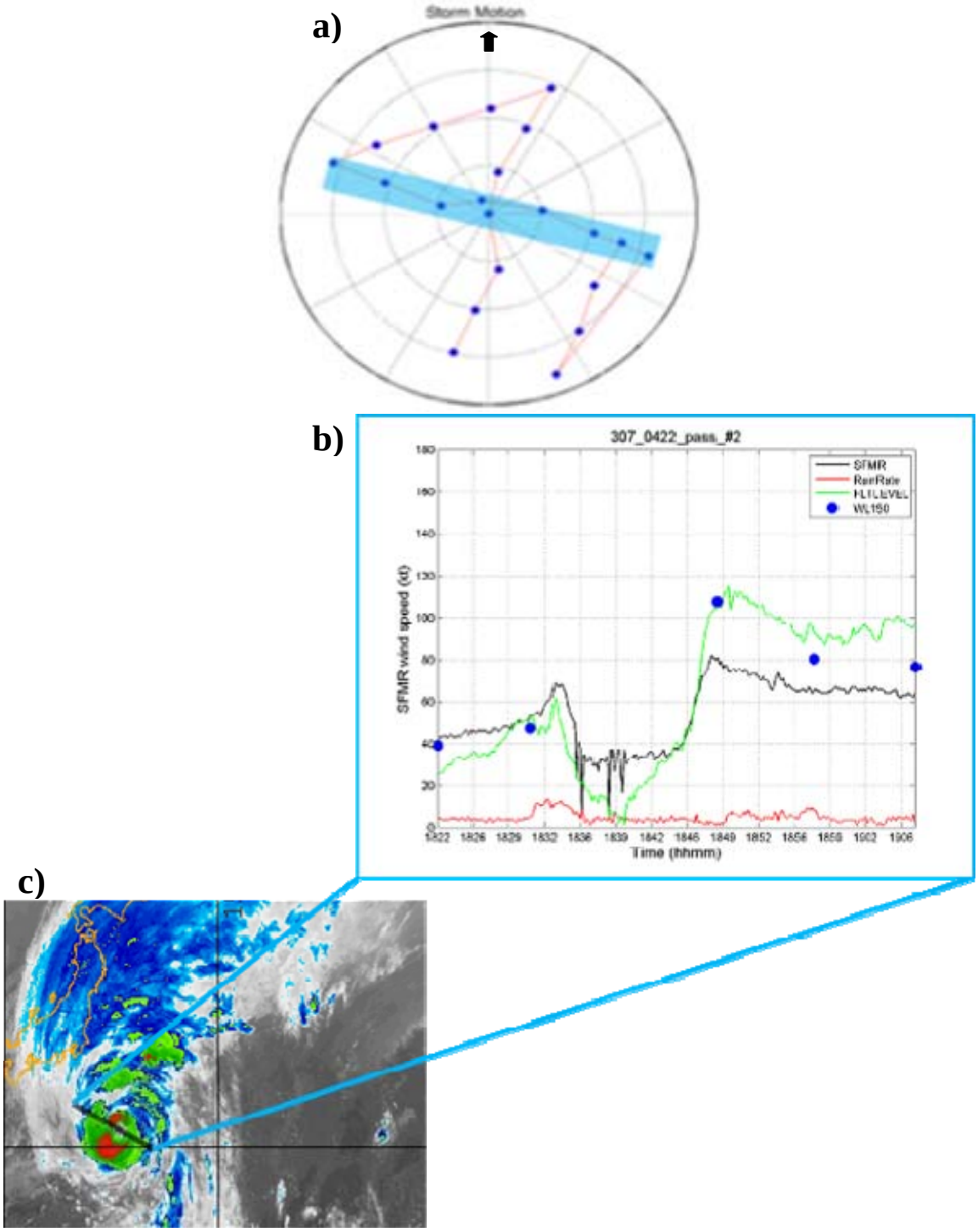

Figure 40. a) Storm-relative motion flight track for flight 0422 in TY Malakas with aircraft pass number two highlighted in blue. b) Cross-section of SFMR and flight-level wind speeds for Malakas flight 0422 pass number two. The WL150 wind speeds calculated for each dropwindsonde in the pass are defined by the blue circles. c) Enhanced infrared geostationary satellite image at the central time of flight 0422. Pass number two is defined by the black line.

3. MEGI

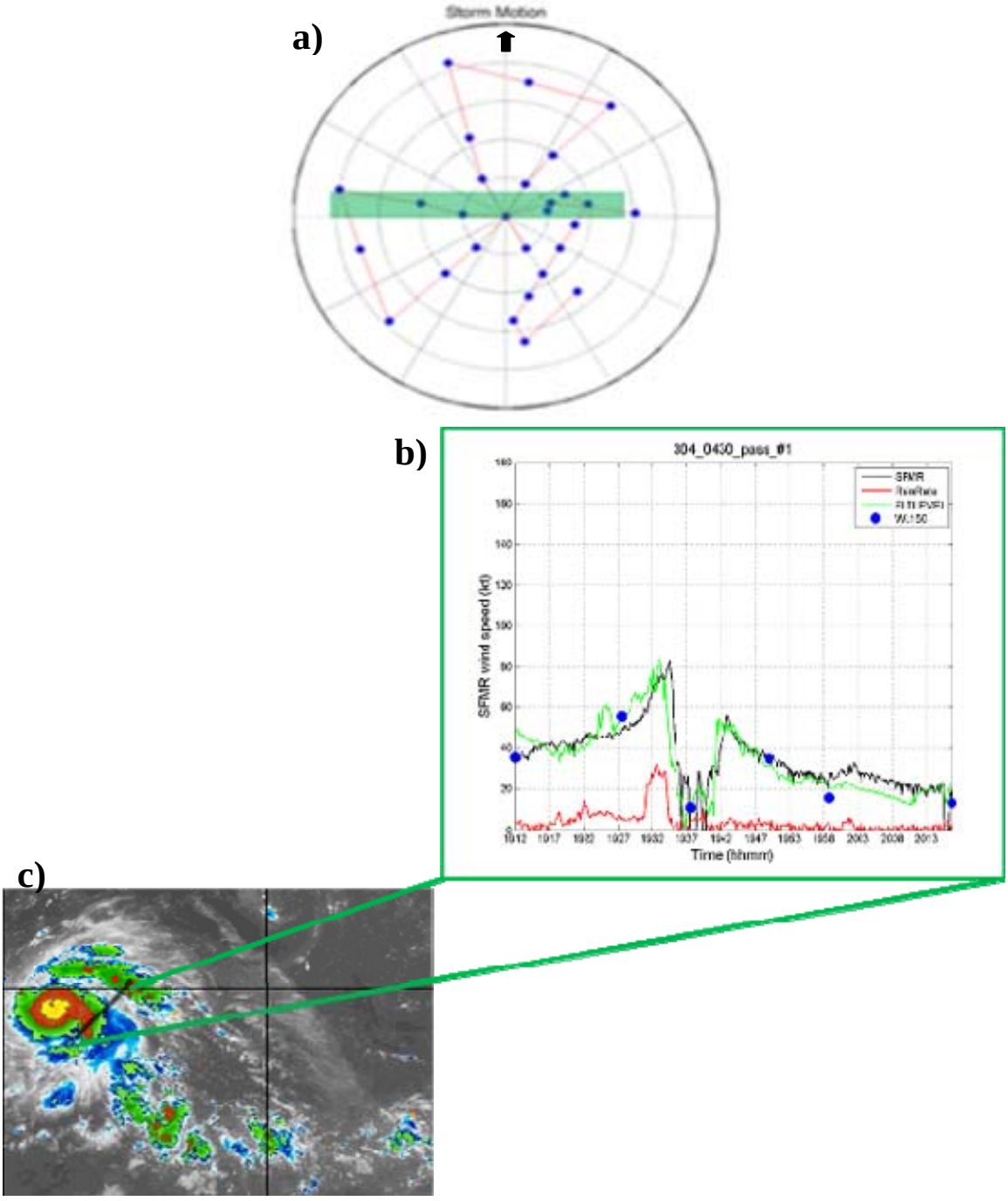

Figure 41. a) Storm-relative motion flight track for flight 0430 in TY Megi with aircraft pass number one highlighted in green. b) Cross-section of SFMR and flight-level wind speeds for Megi flight 0430 pass number one. The WL150 wind speeds calculated for each dropwindsonde in the pass are defined by the blue circles. c) Enhanced infrared geostationary satellite image at the central time of flight 0430. Pass number one is defined by the black line.

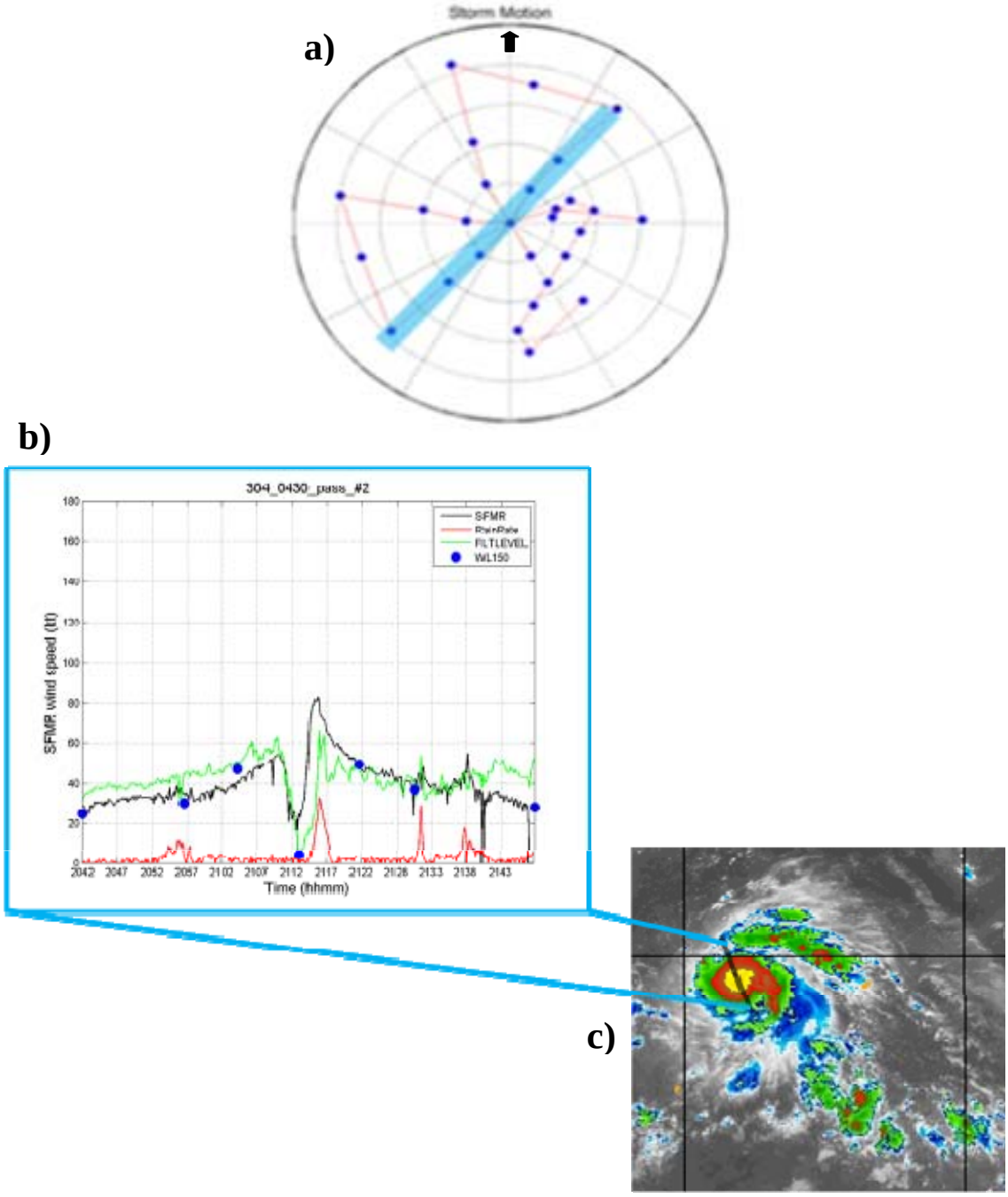

Figure 42. a) Storm-relative motion flight track for flight 0430 in TY Megi with aircraft pass number two highlighted in blue. b) Cross-section of SFMR and flight-level wind speeds for Megi flight 0430 pass number two. The WL150 wind speeds calculated for each dropwindsonde in the pass are defined by the blue circles. c) Enhanced infrared geostationary satellite image at the central time of flight 0430. Pass number two is defined by the black line.

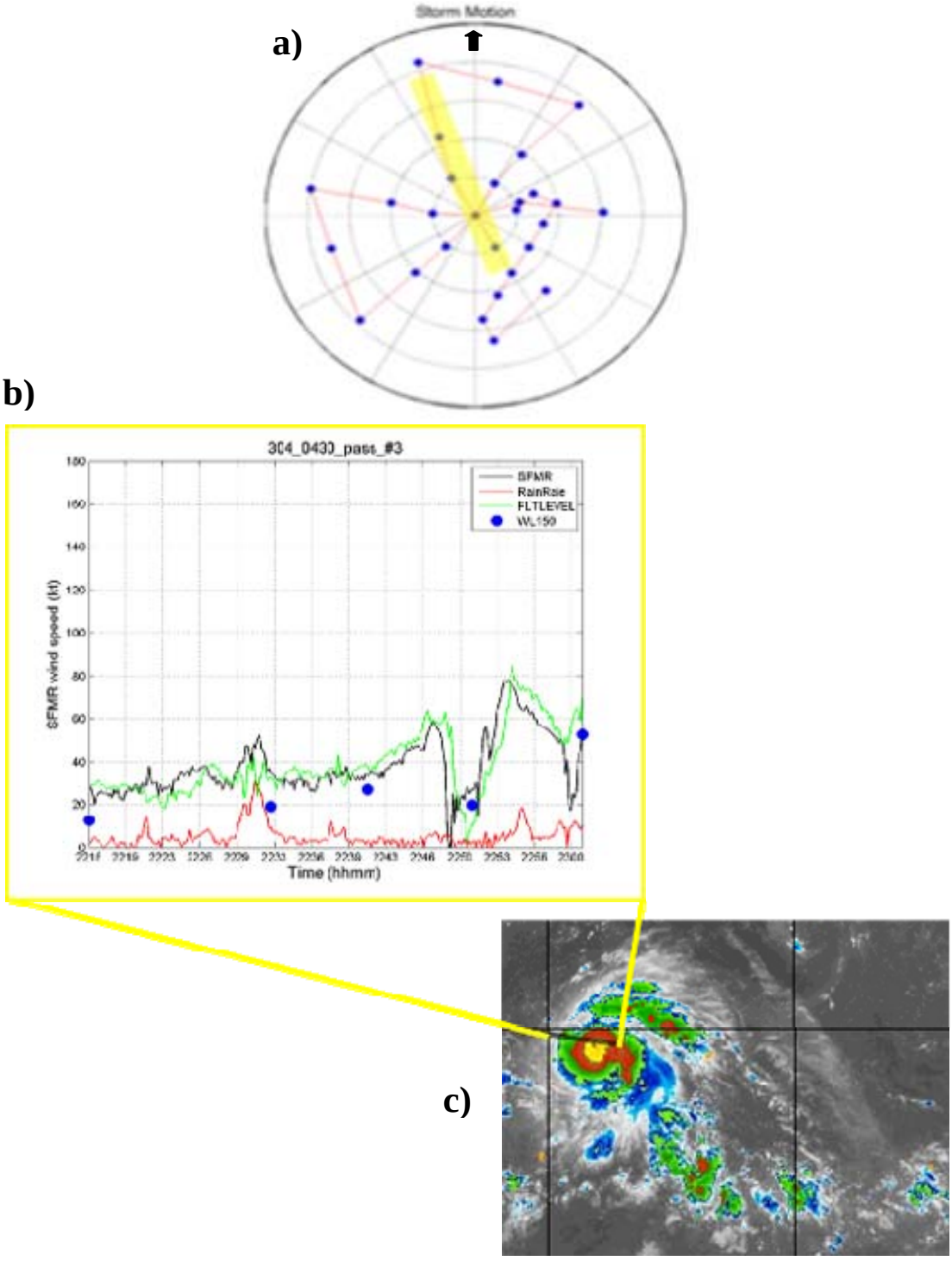

Figure 43. a) Storm-relative motion flight track for flight 0430 in TY Megi with aircraft pass number three highlighted in yellow. b) Cross-section of SFMR and flight-level wind speeds for Megi flight 0430 pass number three. The WL150 wind speeds calculated for each dropwindsonde in the pass are defined by the blue circles. c) Enhanced infrared geostationary satellite image at the central time of flight 0430. Pass number three is defined by the black line.

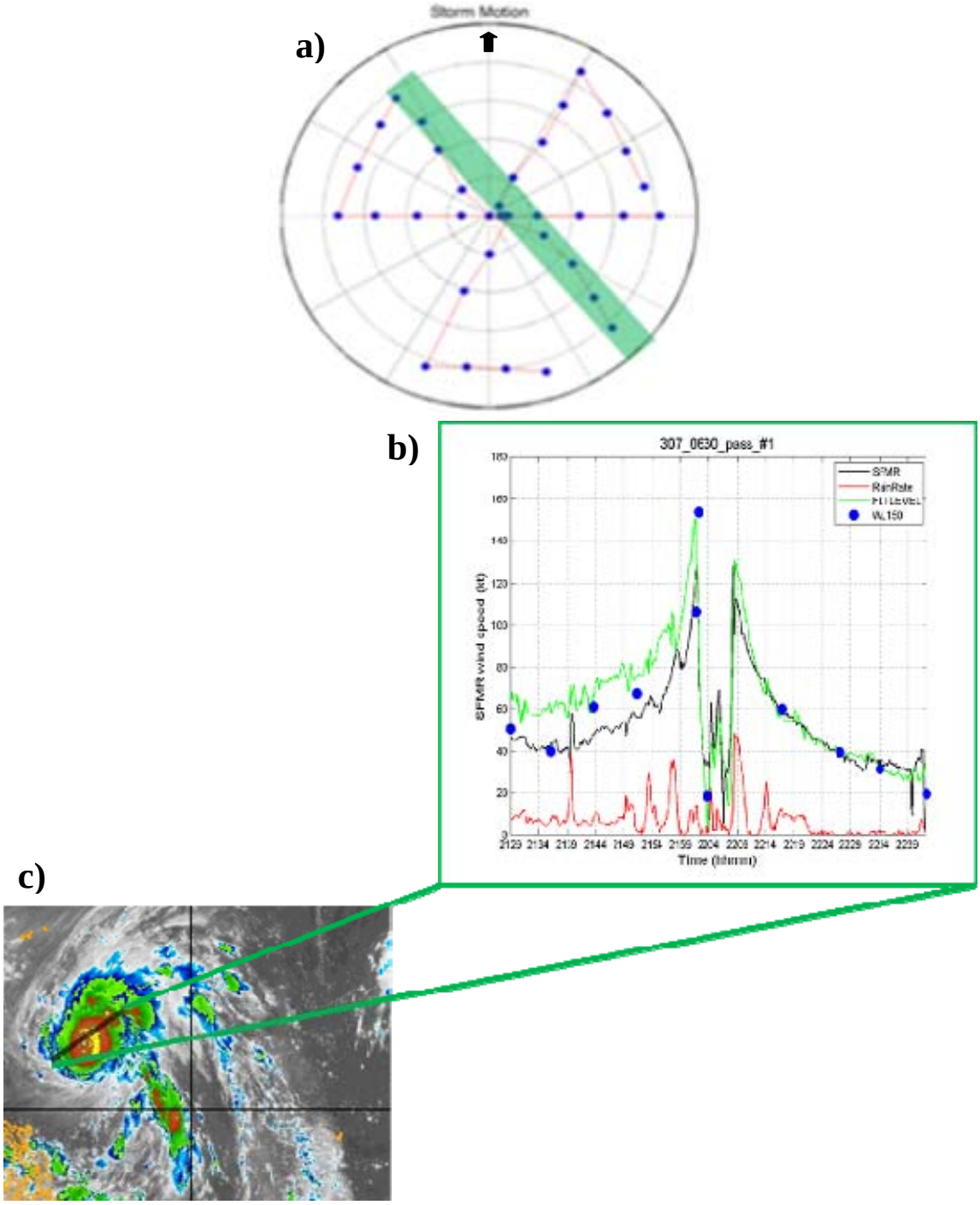

Figure 44. a) Storm-relative motion flight track for flight 0630 in TY Megi with aircraft pass number one highlighted in green. b) Cross-section of SFMR and flight-level wind speeds for Megi flight 0630 pass number one. The WL150 wind speeds calculated for each dropwindsonde in the pass are defined by the blue circles. c) Enhanced infrared geostationary satellite image at the central time of flight 0630. Pass number one is defined by the black line.

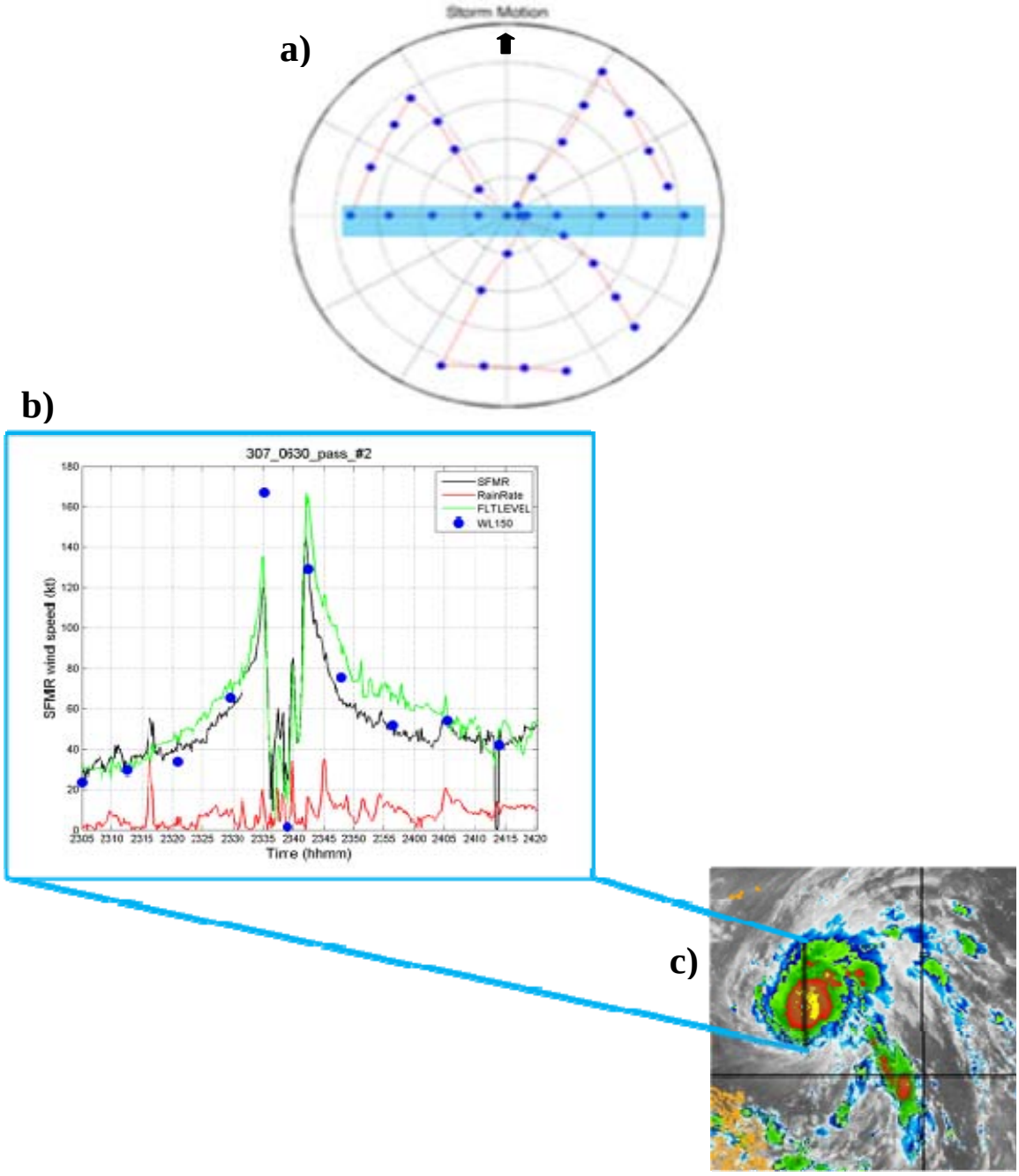

Figure 45. a) Storm-relative motion flight track for flight 0630 in TY Megi with aircraft pass number two highlighted in blue. b) Cross-section of SFMR and flight-level wind speeds for Megi flight 0630 pass number two. The WL150 wind speeds calculated for each dropwindsonde in the pass are defined by the blue circles. c) Enhanced infrared geostationary satellite image at the central time of flight 0630. Pass number two is defined by the black line.

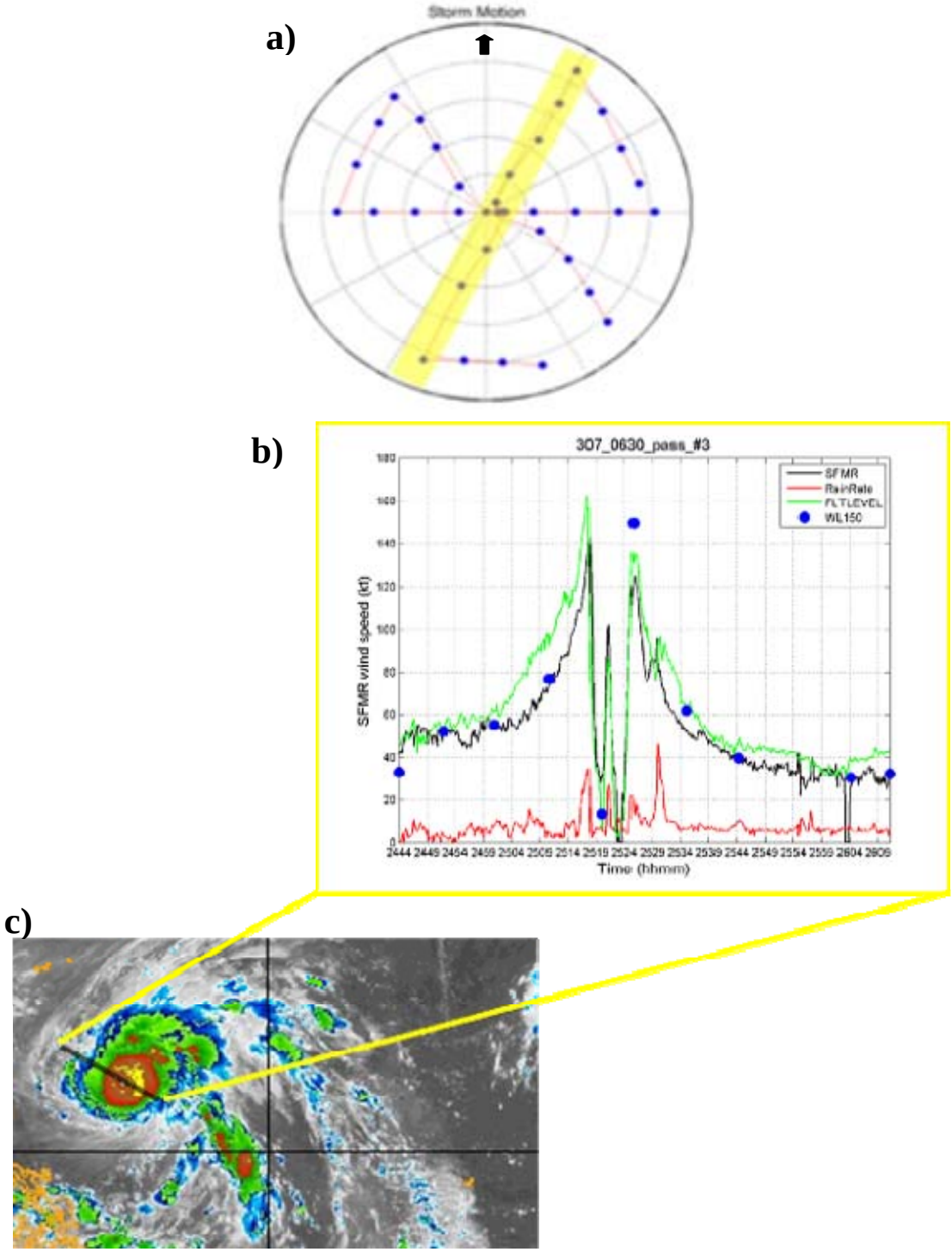

Figure 46. a) Storm-relative motion flight track for flight 0630 in TY Megi with aircraft pass number three highlighted in yellow. b) Cross-section of SFMR and flight-level wind speeds for Megi flight 0630 pass number three. The WL150 wind speeds calculated for each dropwindsonde in the pass are defined by the blue circles. c) Enhanced infrared geostationary satellite image at the central time of flight 0630. Pass number three is defined by the black line.

APPENDIX B. STATISTICAL REGRESSIONS

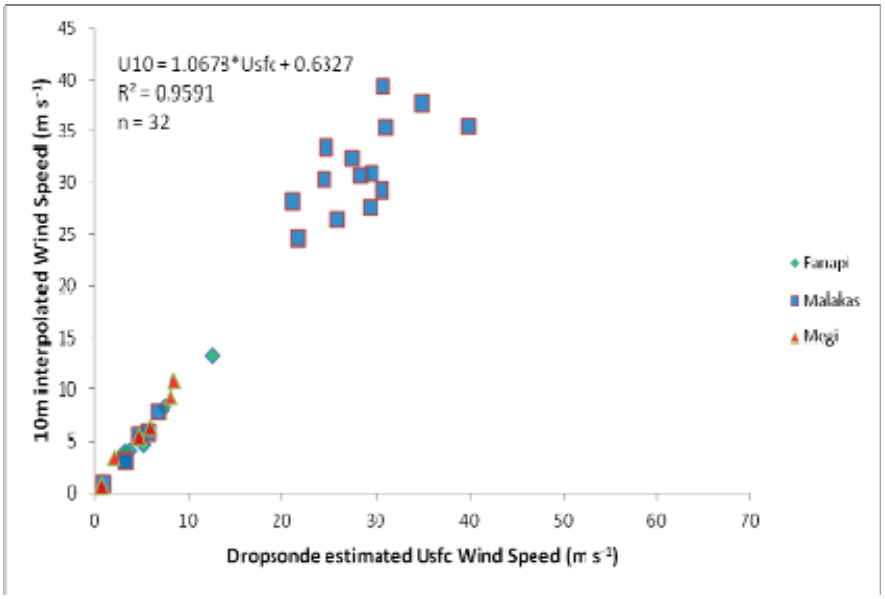

Figure 47. Scatter plot of 10-m and Vsfc wind speeds for the Bin 1 dropwindsondes released more than 5 km inside the RMW.

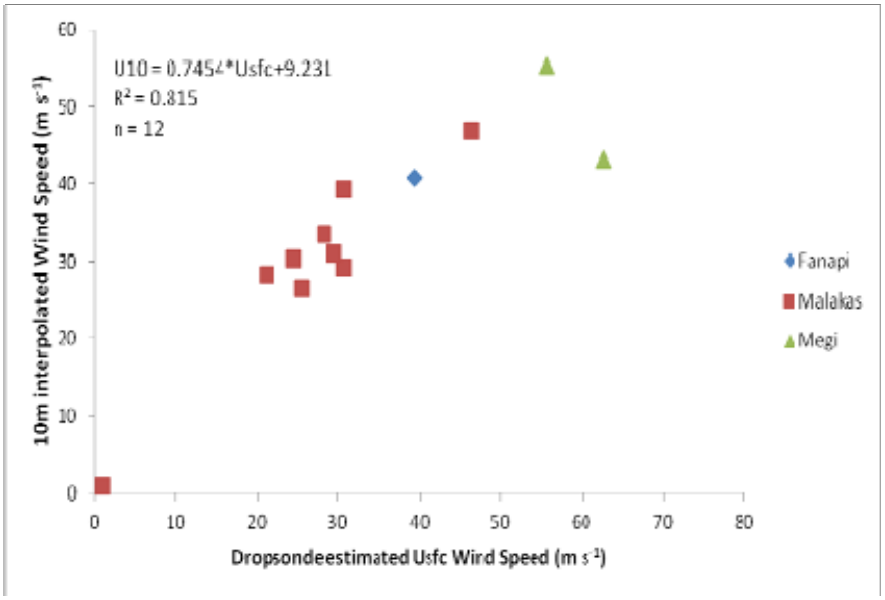

Figure 48. Scatter plot of 10-m and Vsfc wind speeds for the Bin 2 dropwindsondes released within 5 km of the RMW.

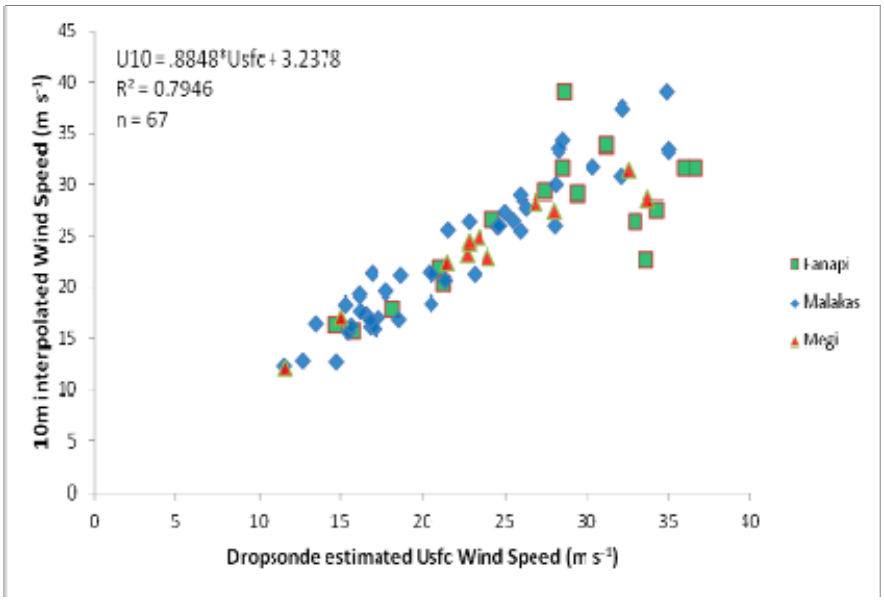

Figure 49. Scatter plot of 10-m and Vsfc wind speeds for the Bin 3 dropwindsondes released in the region between the RMW and three times the RMW.

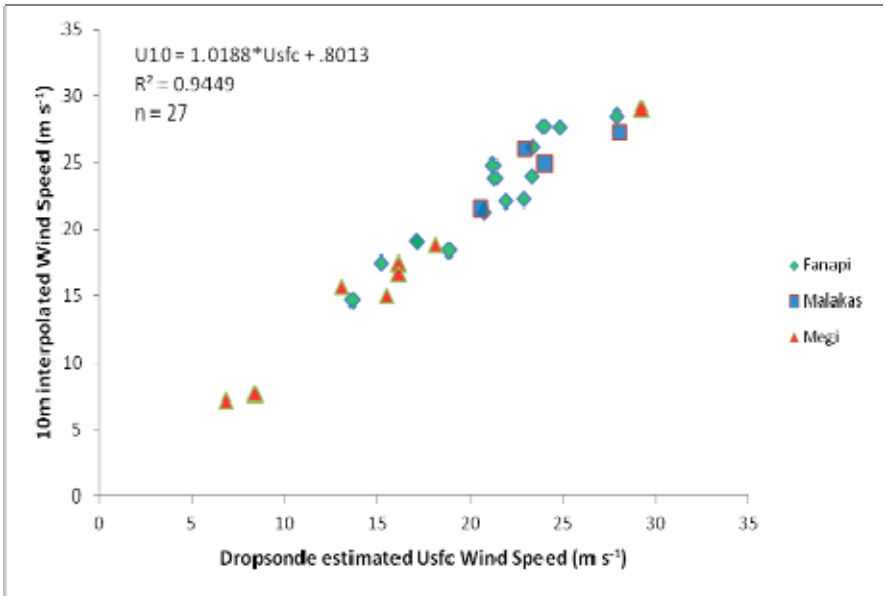

Figure 50. Scatter plot of 10-m and Vsfc wind speeds for the Bin 4 dropwindsondes released in the region between three times the RMW and five times the RMW.

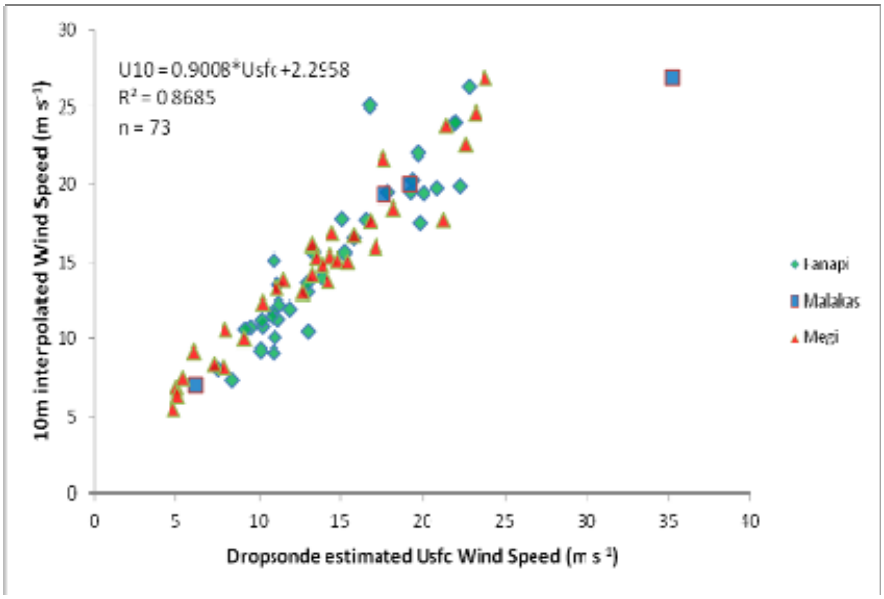

Figure 51. Scatter plot of 10-m and Vsfc wind speeds for the Bin 5 dropwindsondes released beyond five times the RMW.

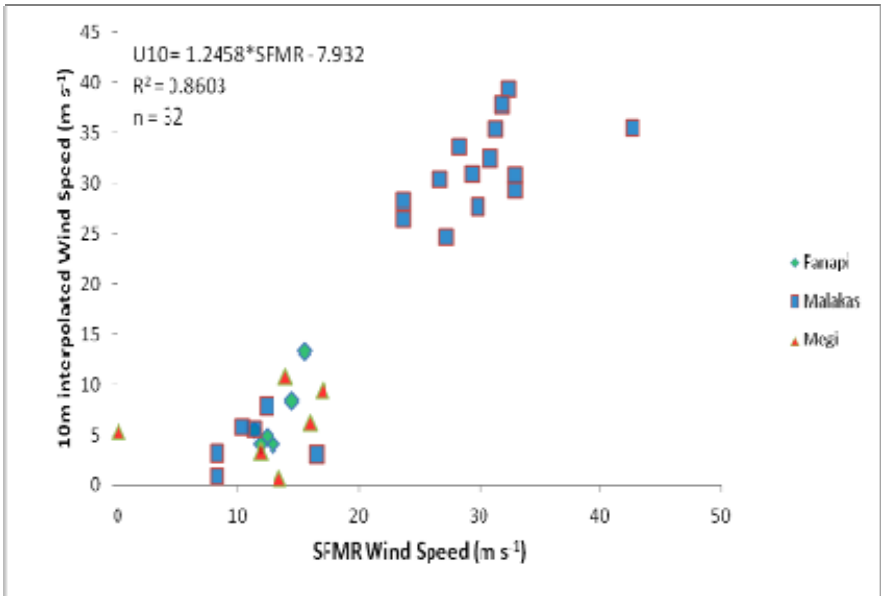

Figure 52. Scatter plot of 10-m interpolated wind speeds and SFMR wind speeds for the Bin 1 dropwindsondes released inside the RMW.

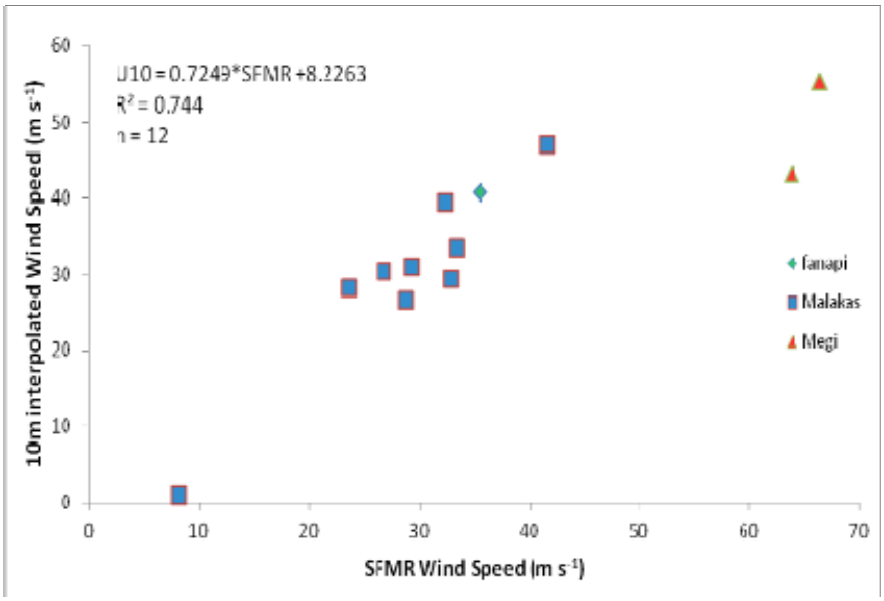

Figure 53. Scatter plot of 10-m interpolated speeds and SFMR wind speeds for the Bin 2 dropwindsondes released within 5 km of the RMW.

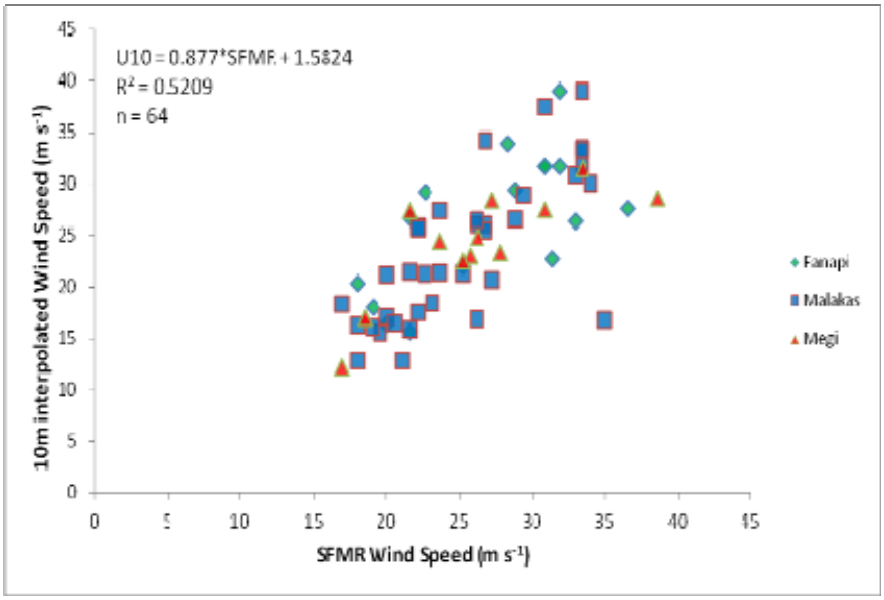

Figure 54. Scatter plot of 10-m interpolated speeds and SFMR wind speeds for the Bin 3 dropwindsondes released in the region between the RMW and three times the RMW.

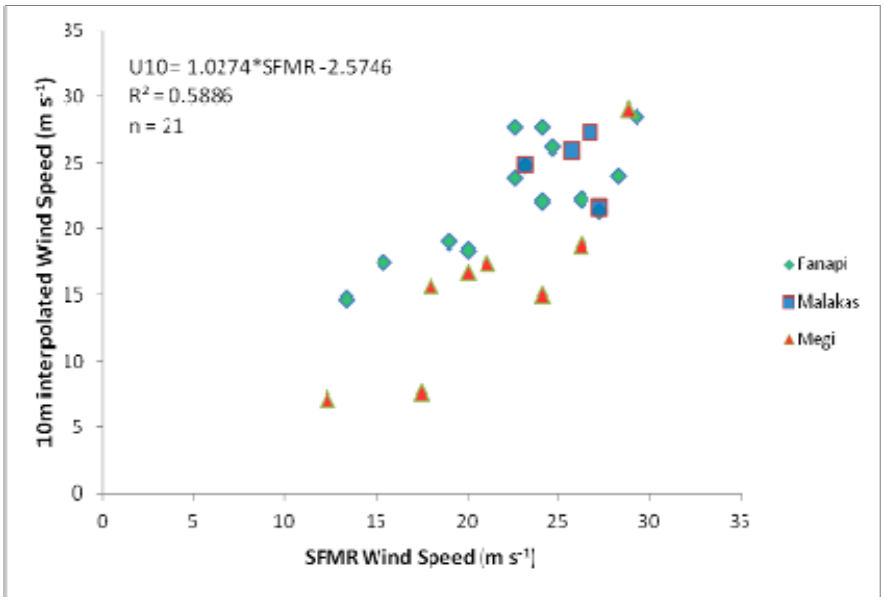

Figure 55. Scatter plot of 10-m interpolated speeds and SFMR wind speeds for the Bin 4 dropwindsondes released in the region between three times the RMW and five times the RMW.

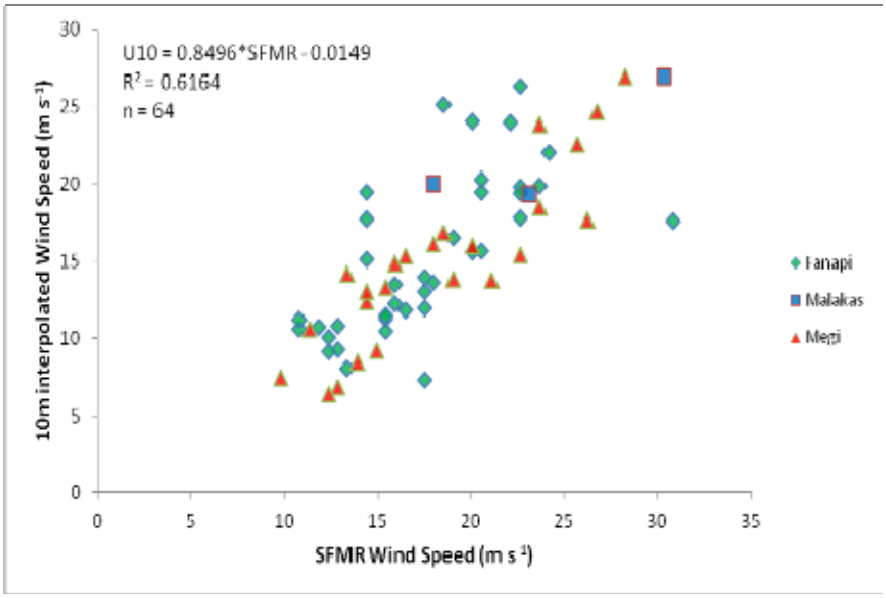

Figure 56. Scatter plot of 10-m interpolated speeds and SFMR wind speeds for the Bin 5 dropwindsondes released beyond five times the RMW.

THIS PAGE INTENTIONALLY LEFT BLANK

LIST OF REFERENCES

Comet Meted UCAR, 2009: Introduction to Tropical Meteorology. [Available online at https://www.meted.ucar.edu/]

Franklin, J.L., 2011: Comments on "Estimating maximum surface winds from hurricane reconnaissance measurements." *Weather and Forecasting,* **26**, 774–776.

____, M.L. Black, and K. Valde, 2003: GPS dropwindsonde wind profiles in hurricanes and their operational implications. *Weather and Forecasting,* **18**, 32–44.

Gray, W. M., 1968: Global view of the origin of tropical disturbances and storms. *Mon. Wea. Rev.,* **96**, 669–700.

Havel, P.J., 2009: Surface wind field analyses of tropical cyclones during TCS-08: Relative impacts of aircraft and remotely-sensed observations. M.S. thesis, Naval Postgraduate School. [Available online at http://edocs.nps.edu/npspubs]

Heck, A.D., 2011: Air-ocean characteristics during the Impact of Typhoons on the Ocean in the Pacific (ITOP) program. M.S. thesis Naval Postgraduate School. [Available online at http://edocs.nps.edu/npspubs]

Hock, T.F., and J.L. Franklin, 1999: The NCAR GPS dropwindsonde. *Bulletin of the American Meteorological Society,* **80**, 407–420.

Impact of Typhoons on the Ocean in the Pacific (ITOP), 2010: ITOP News. [Available online at http://www.eol.ucar.edu/projects/itop/]

Joint Typhoon Warning Center (JTWC), cited 2012a: 2010 Annual Tropical Cyclone Report. Retrieved 17 July 2012. [Available online at http://metocph.nmci.navy.mil/jtwc/atcr/atcr_archive.html]

____, 2012a: 2011 Annual Tropical Cyclone Report. Retrieved 17 July 2012. [Available online at http://metocph.nmci.navy.mil/jtwc/atcr/atcr_archive.html]

Katzberg, S.J., and J. Dunion, 2009: Comparison of reflected GPS wind speed retrievals with dropsondes in tropical cyclones. *Geophys. Res. Lett*., **36**, 1-5, doi:10.1029/2009GL039512.

Powell, M.D., E.W. Uhlhorn, and J.D. Kepert, 2009: Estimating maximum surface winds from hurricane reconnaissance measurements. *Weather and Forecasting,* **24,** 868–883**.**

Uhlhorn, E.W., and P.G. Black, 2003: Verification of remotely sensed sea surface winds in hurricanes. *Journal of Atmospheric and Oceanic Technology,* **20**, 99–116.

____, P.G. Black, J.L. Franklin, M. Goodberlet, J. Carswell, and A.S. Goldstein, 2007: Hurricane surface wind measurements from an operational stepped frequency microwave radiometer. *Mon. Wea. Rev.,* **135**, 3070–3085.

INITIAL DISTRIBUTION LIST

1. Defense Technical Information Center
   Ft. Belvoir, Virginia

2. Dudley Knox Library
   Naval Postgraduate School
   Monterey, California

3. Director
   Joint Typhoon Warning Center
   Pearl Harbor, Hawaii

4. Superintendent
   Naval Research Laboratory
   Monterey, California

5. Professor Patrick Harr
   Naval Postgraduate School
   Monterey, California

6. Director
   Air Force Weather Technical Library
   Ashville North Carolina

7. Professor Russell Elsberry
   Naval Postgraduate School
   Monterey, California